



Contributions of Space Missions to Better Tsunami Science: Observations, Models and Warnings

H. Hébert¹ · G. Occhipinti² · F. Schindelé¹ · A. Gailler¹ · B. Pinel-Puysségur¹ ·
H. K. Gupta³ · L. Rolland⁴ · P. Lognonné² · F. Lavigne⁵ · E. Meilianda⁶ ·
S. Chapkanski⁵ · F. Crespon⁷ · A. Paris¹ · P. Heinrich¹ · A. Monnier¹ · A. Jamelot⁸ ·
D. Reymond⁸

Received: 13 December 2019 / Accepted: 22 September 2020 / Published online: 9 October 2020
© Springer Nature B.V. 2020

Abstract

Most tsunamis occur after large submarine earthquakes, particularly in the Pacific Ocean. However, following the 2004 tsunami in the Indian Ocean, tsunami hazard awareness was significantly raised at the global scale, and warning systems were developed in many other regions, where large tsunamis are rarer but can also produce large catastrophes. Here we first review the basic physics of a tsunami, from its triggering to its coastal impact, and we offer a review of the geophysical and sea-level data that can describe the various processes operating during a tsunami. Global Navigation Satellite System (GNSS) data have a key role in better describing the ground deformation following a tsunamigenic earthquake close to the coast. The GNSS observations complement seismological data to constrain the rupture model rapidly and robustly. Interferometric Synthetic Aperture Radar (SAR) also contributes to this field, as well as optical imagery, relevant to monitoring elevation changes following subaerial landslides. The observation of the sea-level variations, in the near field and during the propagation across the ocean, can also increasingly benefit from GNSS data (from GNSS buoys) and from robust satellite communication: pressure gauges anchored on the seafloor in the deep ocean contribute to warning systems only by data continuously transmitted through satellites. The sounding of ionospheric Total Electron Content (TEC) variations through GNSS, altimetry, or a ground-based airglow camera, is a promising way to record tsunami initiation and propagation indirectly. Finally, GNSS, optical and SAR imagery are essential to map and quantify the damage following tsunami flooding. Satellite data are expected to contribute more to operational systems in the future provided they are reliably available and analysed in real time.

Keywords Tsunami · Early Warning · GNSS · Altimetry · SAR · Ionosphere

✉ H. Hébert
helene.hebert@cea.fr

Extended author information available on the last page of the article

1 Introduction to Current Challenges in Tsunami Science and Warnings

The twenty-first century started with giant catastrophic tsunamis, among them the most massive natural disasters observed in 50 years. Following subduction earthquakes of extreme magnitudes, in 2004 off Sumatra (Indonesia, $M_w=9.1$), and in 2011 off Tohoku (Japan, $M_w=9.1$), tsunami waves were triggered and propagated across the global ocean, after having caused enormous destruction on the local coastal areas, nearshore, and as far as several kilometres inland in some locations. These events were the starting point of a general rise of awareness of this geophysical hazard, which, although known about in a limited scientific community in the 20th century, had very rarely occurred with that level of force since the 1960s.

Tsunamis, which find their origin in geological processes of the Earth, were relatively well understood and characterized in the scientific community before 2004, especially around the Pacific Ocean, where they occur most frequently. Nevertheless, the 2004 and 2011 events surprised most of the tsunami scientific community, essentially because they took place in underestimated, hazardous areas. Indeed, from a physical point of view, any subduction earthquake with a large enough magnitude, shallow depth and significant thrusting component in its focal mechanism, is expected to trigger a tsunami, and available tsunami catalogues underline the tsunami source areas as correlated to subductions (Fig. 1). However, the fact that such extreme earthquakes occurred off Sumatra and of Tohoku was underrated in the beginning of the 21st century, partly because of very long return periods for such events (above 500 years). The subsequent consequences were due to the lack of or the failure of all or part of the basic components of tsunami warning and mitigation, despite being well known at that time (Bernard 2001), i.e. a proper estimation of the geophysical hazard level, an efficient warning system, and a high level of coastal preparedness: in 2004, the lack of regional and national warning systems, and, in 2011, the underestimation of the earthquake magnitude and of the protection design at the Fukushima Daiichi nuclear power plant, in an otherwise well-protected country.

Thus, in 2004 and 2011, the human, industrial and natural coastal vulnerabilities were particularly and tragically highlighted. Yet tsunami science can benefit from favourable conditions which allow the prediction, as soon as the origin has been detected, of propagation times that give sufficient time for preventative measures. This is essentially the basic principle of the tsunami warning, which can be operated mainly for earthquake-related tsunamis. It is worth noting that, by contrast, landslide-related tsunamis cannot often take advantage of the source detection. While regional seismic networks can detect major mass failures, smaller events with significant tsunamigenic potential are challenging to characterize unless local dense geophysical networks are available.

The first regional system was established in 1965 in the Pacific Ocean in the general framework and governance of the UNESCO Intergovernmental Oceanographic Commission (IOC 1965). This organization has strengthened cooperation between systems deployed since the 1940s in Japan and the USA, in the 1950s in Russia, and in the 1960s in French Polynesia (e.g., Kong et al. 2015). In December 2004, seismologists on duty in the Pacific Tsunami Warning Center (PTWC) tried to quickly share information with institutions or authorities in the Indian Ocean. Still, no operational system was in place to address tsunami warnings, the tsunami hazard being underrated at that time. Soon afterwards, the international community had fostered the setting up of Tsunami Warning Systems (hereafter TWS) in every oceanic basin exposed to such a hazard (IOC 2005a,

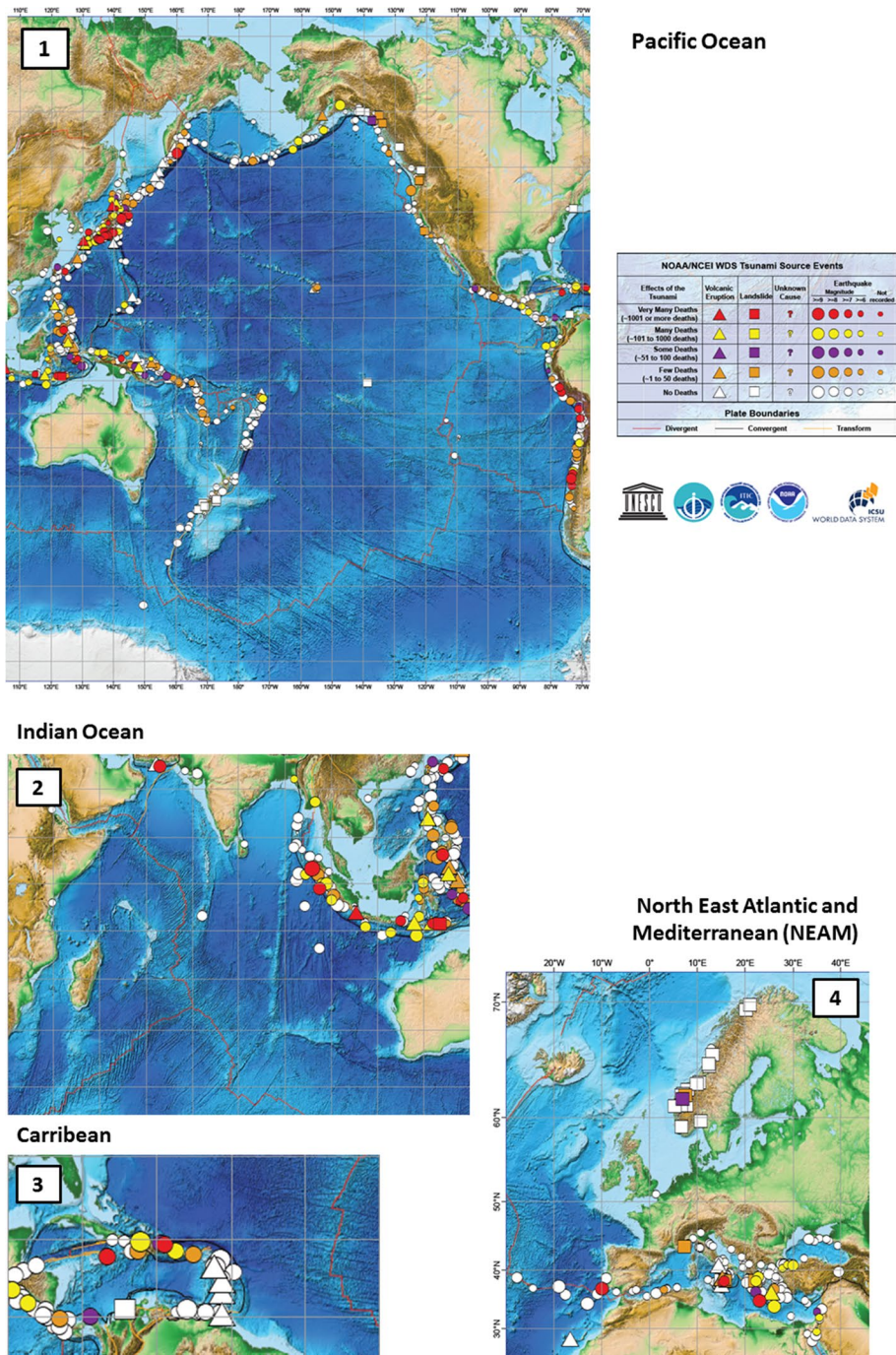


Fig. 1 Map of the major tsunami sources from 1610 B.C. to A.D. 2017, triggered by earthquakes (circles), volcanic eruptions (triangles), landslides (squares), and other causes (NCEI 2017), displayed for the four regions monitored by Tsunami Warning Systems: (1) Pacific Ocean, (2) Indian Ocean, (3) Caribbean and (4) North-East Atlantic and Mediterranean (NEAM) region. Most of the tsunamis are triggered by earthquakes (circles)

b, c). Based on national initiatives and funding, warning systems have been developed in numerous countries and oceanic basins since then.

The different systems are building their capacities and managing the operation procedures through four Intergovernmental Coordination Groups (ICGs). Each of them is responsible for a basin-wide policy (Pacific Ocean, Indian Ocean, Caribbean, North-East Atlantic and Mediterranean Sea) which is built with global interoperability (Fig. 2). For such natural transoceanic hazards, interoperability and data exchanges are naturally essential, and much progress has been made since the 1960s when the Pacific system was in its early stages and when communication means were mostly by fax, phone, and email since the 1990s.

This specific domain of global telecommunication is a prominent topic where satellite usage drastically improved the efficiency of the real-time systems. This, of course, does not constitute the only segment where such data are nowadays vital. In the following examples, we aim to illustrate how space missions significantly contribute to the improvement in tsunami science, especially under the three main headings mentioned above (hazard, warning, mitigation and preparedness):

- Optical imagery may have been the first historical contribution to tsunami science, naturally helping to draw post-disaster surveys and to establish mitigation plans and risk maps. It is often complemented by SAR (Synthetic Aperture Radar) imagery, which also helps to characterize the coseismic deformation, as well as the mapping of coastal damage;
- Altimetry has dramatically contributed to oceanography and oceanic geodynamics since the 1980s. As such a technique maps the oceanic surface, it may be expected to significantly contribute to tsunami remote sensing. However, because of the small number of satellites and the small amplitude of the majority of tsunamis in the deep ocean, it has very rarely proved successful on this issue;

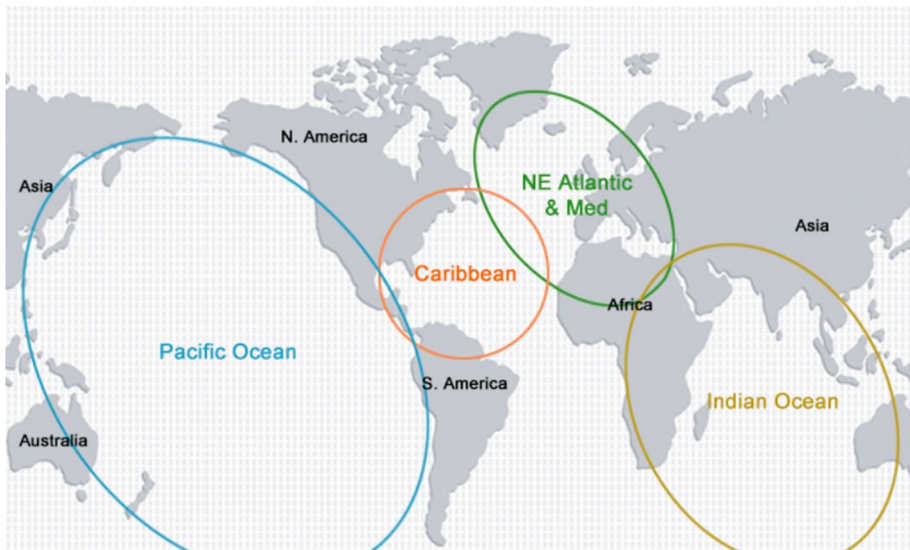


Fig. 2 Areas of the four Intergovernmental Coordination Groups established under UNESCO/IOC framework, following the 2004 tsunami (version from UNESCO/IOC 2008)

- GNSS data (Global Navigation Satellite System, such as Global Positioning System or GPS, Galileo, Glonass, Beidou) are probably among the most important contributors to tsunami science, helping to better map the post-disaster damages and the vulnerable areas with the objective of improving vulnerability assessment and prevention plans, providing more accurate bathymetric data with improved positioning of ship soundings, and, in the event of a tsunami, promptly contributing to a subtle coseismic source imagery and to nearshore measures of sea-level variations. Recently GNSS-reflectometry (GNSS-R) can estimate multiple water height measurements in the case of an optimal GNSS network;
- More recently, the estimation of the variations of the ionospheric TEC (Total Electron Content) (from GNSS, altimetry, airglow camera), due to the coupling of tsunami waves upwards in the atmosphere and ionosphere, has offered convincing pictures of tsunami propagation and may contribute to a promising real-time perspective;
- Hyperspectral data provide a promising way of mapping shallow water depths for numerical modelling dedicated to prevention plans.

Not all these various aspects can be efficient in real-time, depending on how long the data processing and communication means can deliver early information, and the extent to which they rely on ground receivers which are more or less sparsely located. However, they all should play a growing role in the future, not only to improve scientific knowledge but also to contribute to warning and emergency services.

In this paper, we first introduce basic tsunami physics and modelling methods (Sect. 2), then we show how space data increasingly contribute to the tsunami source characterization (Sect. 3), to tsunami height measurements (Sect. 4), and to post event surveys (Sect. 5). Finally we show which selected space techniques can play a growing role in tsunami warning systems (Sect. 6), once they have been validated and made available in real time. Finally we synthesize in the conclusions the maturity level of the different techniques with respect to the various goals addressed, whether scientific, modelling or warning.

2 Basic Physics of Tsunamis

2.1 How a Tsunami is Triggered and Propagates

A tsunami consists of gravity waves propagating across the ocean following a geological event affecting the ocean floor or coastal seafloor, such as an earthquake, a landslide, or a volcanic eruption, all of which can transmit potential energy to the oceanic layer (Fig. 3). The periods of the triggered tsunami waves range from a few tens of seconds (for landslides) to a few tens of minutes (large earthquakes). Their oceanic propagation obeys the gravity wave dispersion equation. The tsunami wavelengths are typically several tens of kilometres that are generated by great earthquakes. This is thus much larger than the water depth (from a few hundred to thousands of metres). In that case, the shallow water assumption leads to a speed $c = \sqrt{gh}$ where g is the acceleration due to gravity and h the water depth.

Propagation of tsunami waves across the oceans takes several hours to more than a day, with velocities reaching 500–800 km/h in the far deep sea or ocean. Tsunami frequency dispersion, especially for smaller wavelengths, corresponds mostly to small landslide sources. Shorter wavelength waves travel slower, and sometimes arrive hours

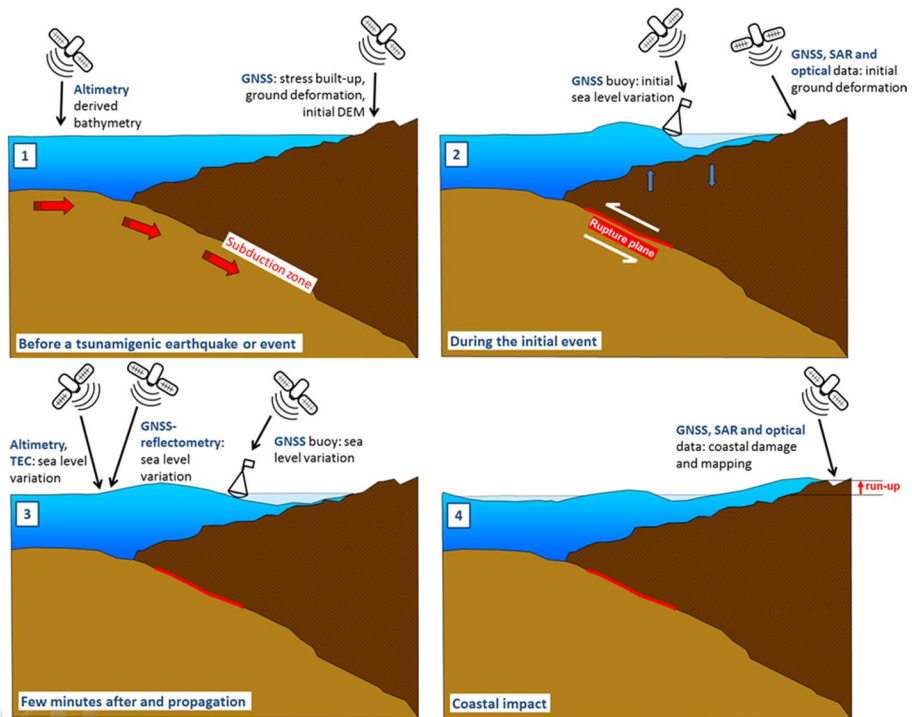


Fig. 3 Different stages of a tsunami following a subduction earthquake, from the stress build-up (1), the coseismic triggering (2), the first minutes after and the subsequent propagation (3), and the coastal impact (4). Each step can be monitored through various space data

after the first arrival at very far distances. The tsunamis with shortest wavelengths, such as those due to landslides, are essentially confined to short distances from the source due to rapid attenuation (e.g., Labbé et al. 2012; Paris et al. 2019).

Tsunamis also trigger perturbations upwards into the atmosphere and subsequently into the ionosphere (Fig. 4). Indeed, tsunami long wavelengths favour a vertical coupling and then propagation of the induced gravity waves in the atmosphere up to the ionosphere, where they in turn induce variations in the TEC (Total Electron Content). The large decrease of the air density with the altitude causes a significantly stronger tsunami-coupled atmospheric wave. Amplified wavefield travels in the ionosphere after coupling between the neutral atmosphere and the ionospheric plasma (e.g., Artru et al. 2005; Occhipinti et al. 2006). The ionospheric record of this upward propagation is made possible by the amplification of the electron density perturbation in the ionospheric plasma at the F-region (at about 200–300 km height). The efficiency of this last coupling strongly depends on the geomagnetic field inclination (Occhipinti et al. 2008): the tsunamigenic perturbation in the F-region plasma is more easily observed at equatorial and mid-latitudes than at the high latitudes. However, where efficient, this underlines how global a tsunami can be, throughout the surface of the oceans as well as in the various atmospheric layers above.

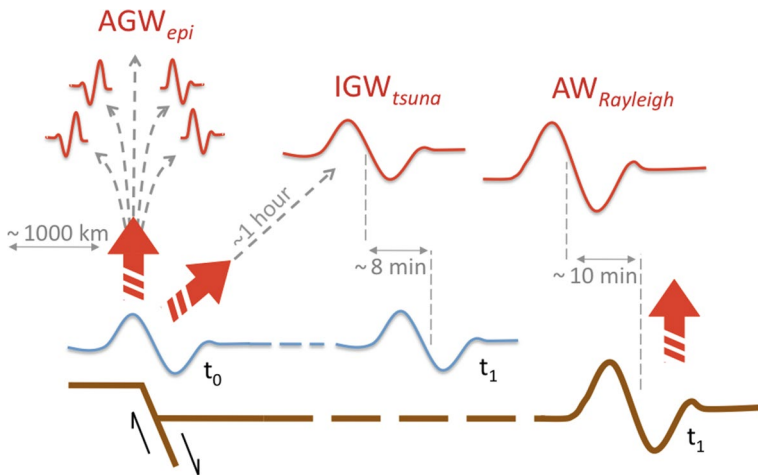


Fig. 4 Atmospheric/ionospheric waves generated by earthquakes and tsunamis: the vertical displacement at the epicentral area or at a teleseismic distance (induced by tsunamis and Rayleigh waves) produces, in the near field, an acoustic-gravity wave coupled with the uplift at the source (AGW_{epi}); in the far-field, an internal gravity wave coupled with the tsunami (IGW_{tsuna}), and a pure acoustic wave coupled with the Rayleigh wave ($AW_{Rayleigh}$). During the upward propagation, the AGW_{epi} , IGW_{tsuna} and $AW_{Rayleigh}$ are strongly amplified by the effect of the exponential decrease in the air density with increasing height (from Occhipinti 2015)

2.2 Spatial and Time Scales of a Tsunami

This basic review of a tsunami's life indicates that various temporal and spatial scales are at play during the event. While the original source takes a few minutes to couple with the oceanic layer, and implying dimensions from several hundreds of metres to more than a thousand kilometres at most, the subsequent propagation involves hours of sea-level variations over distances exceeding several thousands of kilometres (in some cases related to large earthquakes) while tsunamis initiated from landslides propagate only a shorter distance.

While the tsunami offshore propagation is characterized by wave amplitudes smaller than one metre in most cases, the nonlinear amplification close to the coasts leads to very large wave amplitudes, damaging the coastlines and sometimes reaching as far as several kilometres inland. The powerful flow of water flooding, arriving on the coast with velocities from 20 to 40 km/h, is responsible for the serious destruction of vulnerable buildings and facilities. It is able to cause casualties as soon as the water height is greater than about 50 cm, and also to reach several kilometres inland for the largest tsunamis.

2.3 Modelling Approach

Tsunami hazards can be efficiently studied through numerical methods that have considerably improved since the first developments in the 1980s. The tsunami wavelengths are large compared to the water depth (several hundreds of metres) in most of the different stages of the tsunami's life. The initiation is begun by an instantaneous coupling of the ground

deformation with the oceanic layer, which is usually computed with a classical elastic model (e.g., Okada 1985) taking into account the seismological parameters of the rupture.

Numerical methods, generally based on finite differences or finite element schemes, have mostly been developed using the shallow water assumption, which can also account for nonlinear terms close to the shore (e.g., Synolakis and Bernard 2006). Under the shallow water approach, there is a direct relationship between the tsunami velocity c and the water depth h , through $c = \sqrt{gh}$ where g denotes the acceleration due to gravity. The propagation grid is therefore composed of the wave velocity converted from the water depth at each grid cell. To account for the nearshore amplification and wave shoaling, the grid resolution should increase close to the shore, requiring finer bathymetry. Eventually, the computation of the possible run-up values requires a fine DEM (Digital Elevation Model) of the ground in the case of flooding.

As for landslide sources, the processes are more complex to model, and various methods have been developed, first with the sliding of solid blocks, or with fluid-like flows with various rheologies. While 3D Navier–Stokes equations for complex flows should be used (e.g., Abadie et al. 2012), these numerical methods are usually costly. Thus, most of the methods use 2D depth-integrated approaches, when it is relevant (e.g., Heinrich et al. 2001; Løvholt et al. 2015), with constant viscosity, or depending on the flow dynamics such as shear stress evolution (Assier-Rzadkiewicz et al. 1997); internal friction laws for granular flow can also be applied (Mangeney et al. 2000).

The coupling with water waves requires addressing frequency dispersion induced by the short wavelengths of the triggered tsunami waves, as observed in various experiments (Fritz et al. 2004, Mohammed and Fritz 2012), and handled by solving weakly nonlinear Boussinesq equations (e.g., Glimsdal et al. 2013). Numerical methods addressing both the landslide and the wave propagation are efficient for case studies, either for past or recent events (Poupardin et al. 2017) and/or for hazard scenarios (Paris et al. 2019).

While numerical modelling has been crucial in better estimating tsunami hazards, very detailed bathymetric and topographic data are required to accurately simulate coastal amplification. In addition, the parameters input into the models also need fine characterization of the geophysical source. In the following section, we shall show how space data can contribute to all these various aspects.

3 Contributions of Space Data to Improved Tsunami Source Assessment

Tsunami hazard prevention partly relies on numerical modelling which has been greatly improved in recent years, not only thanks to high-performance computing, but also to more accurate bathymetric and topographic data, some of which is directly derived from satellite data. However, one should not forget that numerical techniques should be controlled in their various steps, using robust data, validated schemes and keeping in mind their uncertainties. One point is to rely on validated benchmarked problems (and their progress is constantly noteworthy, e.g., Synolakis and Bernard 2006; Lynett et al. 2017); another point is undoubtedly to enter the correct data and parameters into the models. In addition, a tsunami results from the coupling between a specific submarine ground deformation, and the overlying oceanic layer. Thus, two distinct layers (crust and ocean) need to be scrutinized in order to gather data describing the physical processes involved. Space missions can help to address this challenge—to better understand the initiation, the propagation, and the

flooding related to a given tsunami. In this section, we introduce the main techniques used nowadays to characterize tsunami source, independently from their possible operational use addressed in Sect. 6.

Hazard studies first need a relevant description of tsunami sources, based on catalogues and/or syntheses of recent well-documented events. The fact that hazard studies may be conducted under deterministic or probabilistic approaches is not discussed in this paper, since both need the same kind of data anyway. Then a fine description and measurement of tsunami heights area is needed to better describe the propagation pattern and validate the models. Finally, identifying hazardous coastal areas requires the establishment of observational databases in the aftermath of tsunami flooding, or based on paleotsunami studies.

3.1 Study of the Seismic Cycle and Plate Coupling to Design Possible Tsunami Sources

Earthquakes are not predictable at the present time. However, a number of techniques based on satellite geodesy (GNSS, SAR) allow the monitoring of specific fault areas and seismogenic zones in order to better understand processes possibly linked to the trigger of seismic ruptures. Significant advances have been made since the 1990s in various seismically active areas (see Elliott et al. 2016; Gupta and Gahalaut 2015). Studies from satellite geodesy contribute to a better understanding of the different stages of the seismic cycle and offer a way to monitor the deformation rates, including time-dependent phenomena, such as slow slip events or transients that are observed in subduction zones and that are probably related to seismogenesis.

For submarine seismic areas, satellite geodesy naturally only gives a partial subaerial view, but is possibly also relevant for detailed coastal processes (e.g., Polcari et al. 2018). However, active submarine coseismic areas can also be monitored through a growing number of sensors, including ocean bottom seismic arrays, submarine cables (Howe et al. 2019), acoustic ranging submarine geodesy and promising optical fibre (Ajo-Franklin et al. 2019; Sladen et al. 2019), defining the so-called seafloor geodesy. Though primarily based on submarine networks, most of the methods use kinematic GNSS satellites to be tied to the global reference frame, and they provide promising insights into the estimation of accurate seafloor deformation, including some possible signals close in space and time to the largest tsunamigenic ruptures, such as in 2011 in Tohoku (Bürgmann and Chadwell 2014).

3.2 Characterization and Extent of the Rupture for an Earthquake

Following an earthquake, seismic networks at regional, national and global scales rapidly define the location, depth and magnitude of the event. However, the magnitude, location and depth of the earthquakes are not sufficient to characterize the tsunami hazard. This must be complemented with information on the rupture extent (whenever it was potentially submarine) and pattern (whenever it involved a dip slip component to efficiently couple with the oceanic layer). Seismology is able to provide such information, although the ambiguity on the double couple resolved through seismic tensor inversion does not define the accurate fault mechanism, unless local tectonics is well known, as in typical subductions, a task that is sometimes difficult under the sea.

The elastic deformation and the crustal rupture due to an earthquake imply significant ground deformation that can be measured by satellite data. The recent progress made in the GNSS data processing offers the more plausible and precise technique allowing for a

quick computation of a ground deformation map/picture and thus the ability to extrapolate the possible extent of the rupture beneath the sea, depending on the rupture duration and GNSS network location and density close to the rupture zone. Such data contributes to joint inversions providing a finer pattern for the rupture and contributing to magnitude estimates (see, for example, for recent tsunamigenic earthquakes, Ozawa et al. 2011; Wang et al. 2013; Grandin et al. 2016) in addition to giving interpretation of the successive ruptures within the seismic cycle of a subducting plate (Moreno et al. 2010). GNSS data also bring constraints on the post-seismic sequence following tsunamigenic ruptures (Raharja et al. 2016), even in the specific case of slow earthquakes that produce tsunamis much larger than the magnitude level indicates, as in the case of the Java 2006 earthquake and tsunami (Hébert et al. 2012).

Interferometric SAR imagery analysis also gives valuable information for the coastal deformation induced by an earthquake, though in general offering only a truncated view since the technique does not reveal the seafloor deformation. In specific cases, such as in narrow bays surrounded by subaerial ground, this applies admirably, as in the recent Palu, 2018, earthquake and tsunami (Jamelot et al. 2019). As GNSS data, such ground deformation data can thus be inverted in terms of source pattern characterization.

However, recent major tsunamigenic earthquakes could not all be easily monitored through GNSS or InSAR data, being located far from coastal ground places where these techniques are able to provide measurements (Ammon et al. 2008; Lay et al. 2010), and seismological methods remain unavoidable and quite unique in these cases too. Only seafloor geodesy could complement ground-based GNSS data there.

Finally, the recently developed ionospheric seismology has been supported by the growing number of GNSS networks allowing for imaging the TEC variations induced by the seismic shaking. In the case of submarine tsunamigenic earthquakes, this technique brings an original view of the various processes occurring in the near field, during the minutes when the tsunami is initiated. This concept will be developed in Sect. 4.

3.3 Identification of Tsunamigenic Landslides

Landslide-prone sections in coastal places can also be monitored, using not only dense seismic arrays and tilt meters but also satellite methods as well. Geodetic techniques, including space borne and ground-based SAR data, are currently common methods of monitoring active volcanoes, as well as for major landslides threatening valleys (e.g., Gaffet et al. 2010; Carlà et al. 2019b). The data provides information on the ongoing ground deformation, which can be compared to mechanical models, and it also possibly contributes to operational warning when case values exceeding relevant thresholds are detected, such as on Stromboli (see Sect. 6).

In addition to GNSS and SAR methods useful to estimate ground deformation, the computation of differential DEM through ground space image matching (e.g., Guérin et al. 2014) also estimates change detection and helps to monitor landslide and slope deformation prior to collapses that can be tsunamigenic when they are at the coast. From that perspective, the recent study of the 2017 Greenland collapse and tsunami allowed the identification of a suspected possible rock volume (Fig. 5) that could be destabilized in the vicinity of the previous tsunamigenic failure in 2017, which produced flooding in a village approximately 30 km away from the source (Paris et al. 2019). Such a volume was consistent with estimates made from the analysis of seismic waveforms (Bessette-Kirton et al. 2017; Chao et al. 2018).

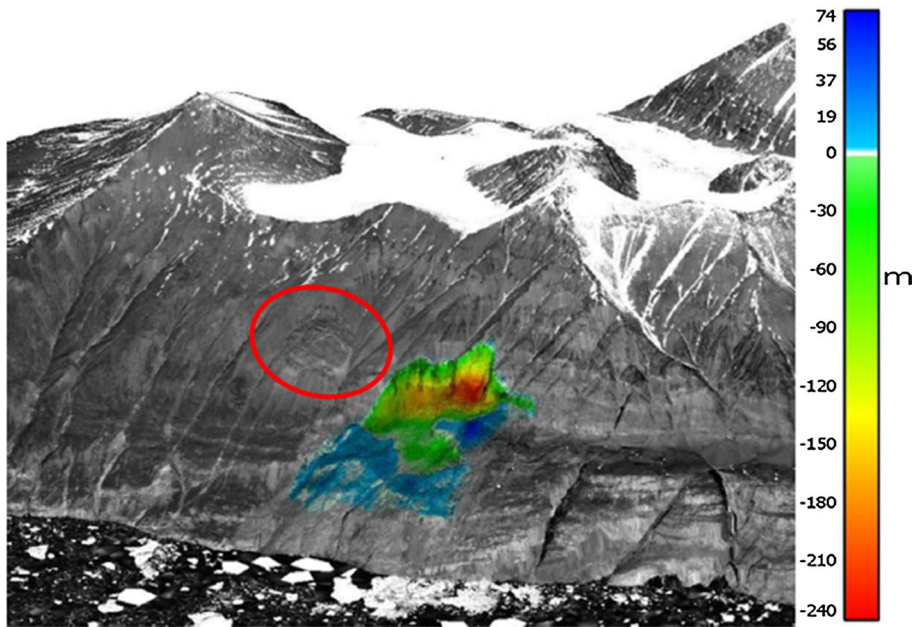


Fig. 5 Following the 2017 landslide and tsunami in western Greenland, difference between the “before” (Spot6 2013) and “after” (Pleiades 2017) digital surface models (DSM), superimposed on the “after” DSM, computed from the Pleiades tri-stereoscopic images from 2017. The variations of the difference elevation values (in m) are represented with the colour bar. The red ellipse indicates a potentially unstable area exposed to possible future failure (Figure adapted from Paris et al. 2019)

However, many tsunamigenic landslides have their origins solely on the seafloor, for which context very few detailed maps are generally available. In some cases, seismic or hydroacoustic networks operated in the near field are able to record seismic signals due to the destabilization and sliding of the volume on a rough interface (e.g., Caplan-Auerbach et al. 2001). But generally high-resolution bathymetric data available prior to and after the event naturally help to better characterize the landslide shape and volume, as in the recent case of the 2018 Krakatau submarine collapse (Paris et al. 2020), complemented by satellite optical or SAR imagery for the subaerial portion (Ye et al. 2020). As proper data are generally only available for intermediate or shallow depths, altimetry derived bathymetry is not of much use, and only high-resolution sounding data from ships can provide the necessary information.

3.4 Bathymetric and Topographic Data Requirements for Numerical Modelling

Initial attempts to model tsunami propagation relied on ray theory derived from geometrical optics and accounting for diffraction when strong velocity gradients occurred. For that purpose, the first global bathymetric datasets, derived from marine cruises and thus only roughly accounting for seafloor details (Smith 1993), were used in the first numerical methods which proved very useful to compute tsunami arrival times and to examine the first order amplifying bathymetric patterns (Satake 1988; Mader and Curtis 1991). The development of global bathymetry derived from satellite altimetry (Smith and Sandwell

1997) at that time provided strikingly more detailed maps from the ocean seafloor, and thus further enabled a more ocean-wide and accurate coverage, useful for tsunami numerical models (Titov and González 1997; Hébert et al. 2001).

Nonlinear effects leading to increased tsunami impacts along the coast require finer bathymetry close to the shore to constrain numerical models, whereas altimetry derived datasets are out of their validity domain. Such shallow bathymetry can be evaluated through the inversion of ocean wave refraction by innovative methods (Poupardin et al. 2014; Li et al. 2016). Although direct local measurements using airborne LIDAR are now contributing to very high-resolution datasets (for example the Litto3D® project in France), methods based on satellite hyperspectral data also offer an interesting perspective (Ma et al. 2014).

Merging fine bathymetry with fine low topography is essential to make tsunami modelling robust in coastal areas. Generally, tsunami models provide accurate estimations only when using grid cell sizes typically consisting of a few metres. Recent advances on the acquisition of coastal datasets, with a large numbers of methods (see, for example, Salameh et al. 2019, for a review) indicate that such models should be more and more robust in the areas at risk, and much more useful to tsunami hazard studies, not only for better preparedness, but also from the perspective of computing real-time forecasting (see Sect. 6).

4 Measuring Tsunami Wave Heights and Periods

Once the tsunami has been generated, it is able to propagate for hours, and to produce damaging impact thousands of kilometres away from its source. Transoceanic propagation is currently essentially monitored through conventional tide gauges in harbours, and, in the deep ocean, through deep ocean pressure gauges (such as the Deep Ocean Assessment and Reporting of Tsunamis, DART, Milburn et al. 1996). These data, complemented by tide gauges deployed in harbours, are the key sensors providing the physical features of the tsunami wave trains.

4.1 Importance of GNSS Data for Sea-Level Measurement Techniques

The network of usual tide gauges deployed in harbour areas was considerably developed on a global scale after the catastrophic 2004 tsunami (Angove et al. 2019), and sensors were also improved. Indeed, most of the coastal sea-level gauges now consist of radars which avoid floating devices and management of probing tubes in the sea, the way most tsunamis were measured in the past (e.g., Hébert et al. 2007, in La Réunion island).

In addition, at some distance from the coast, where measurements can be conducted on buoys and anchored devices, new gauges have been developed based on GNSS data. For example, Japan developed the GNSS buoy system during the late 1990s (Kato et al. 2010; Terada 2015) (Fig. 6 top). This tsunami monitoring system uses Real-Time Kinematic GPS technology to position a GNSS receiver mounted on top of a buoy, floating at the sea's surface, in relation to a land-based GNSS receiver, thus taking advantage of differential processing. After various successful experimental systems, in 2008, the Nationwide Ocean Wave information network for Ports and HARbourS (NOWPHAS 2020, Japan) was originally established with 10 GNSS buoys (extended to 18 sensors as of 2019), mostly along the Sanriku coast, an area identified as being prone to frequent and large tsunamis.

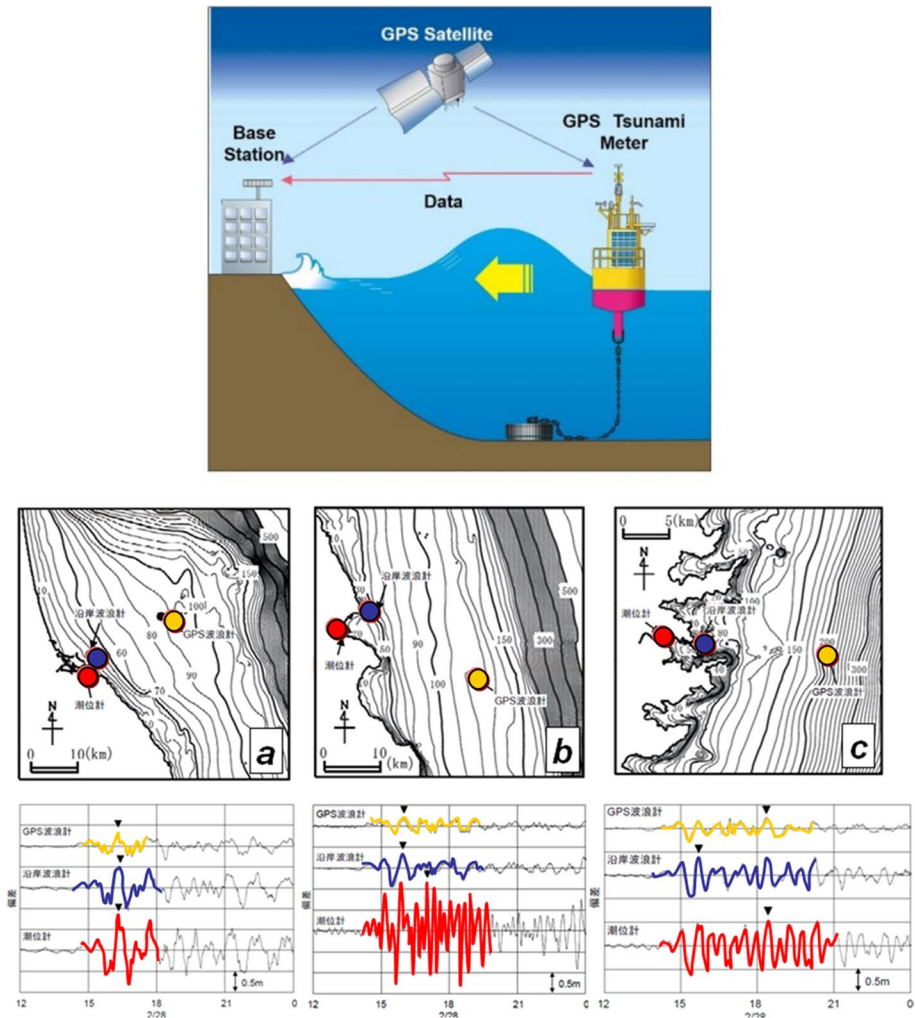


Fig. 6 Top: device on GNSS buoys deployed nearshore (figure taken from Kato et al. 2018). Such a buoy off Iwate prefecture was able to detect an unexpected 7 m high wave, 24 min after the March 2011 Tohoku earthquake, allowing for an updated warning level 4 min later (Ozaki 2012). Bottom: Subsets a, b and c show the deployment of such GNSS buoys (yellow dots) to complement conventional tide gauges located at the entrance of the bay (blue dots) and the bottom of the bay (red dots), for three different bays in north Japan (from Kawai et al. 2012). Different amplifications are evidenced for the tsunami coming from the Chile 2010 earthquake, about 22 h after the triggering, and showing different kinds of site effect amplification depending on the bay

These sensors also contribute to refined studies on the coastal amplification response to a tsunami arrival. For instance, the tsunami generated by the February 2010 Chilean earthquake was recorded on the Japanese coast after a 22-h propagation time, on tide gauges and GNSS buoys (Kawai et al. 2012) (Fig. 6 bottom). The data record illustrates how the tsunami amplification takes place on three different bays, and a quantification of the amplification factor (that also probably depends on the frequency) is enabled: each bay exhibits a

specific site effect, related to its dimensions and depth. A better identification of these various coastal amplification patterns obviously plays a key role for the improvement in hazard estimation.

4.2 Satellite Altimetry

Due to their global coverage and continuous measurement, altimetry satellites have been considered to detect tsunami waves since the 1990s. Indeed such techniques aimed at studying the oceanic surface could intuitively produce useful data to monitor tsunami heights. However, the very small tsunami amplitudes expected in the deep ocean made the investigation very uncertain, since the altimetry signal is much hidden in mesoscale oceanic processes. The latter, however, usually implies spatial scales larger than those of tsunami waves, which can therefore be extracted as short wavelengths. A tentative detection was proposed during the 1992 Nicaragua tsunami, which was supported by tsunami numerical modelling (Okal et al. 1999).

In 2004, the detection was very impressive since the raw altimetry signal clearly exceeded the mean oceanic ambient signal and thus provided a crest-to-trough displacement amplitude of 80 to 100 cm on Topex/Poseidon and Jason platforms (Occhipinti et al. 2006) (Fig. 7), observed about 2 h after the earthquake. These outstanding data were also unique for the further investigation of seismological interpretation, since their inversion gave a picture of the slip distribution for the 2004 Sumatra earthquake, which proved very consistent with other geophysical inversions (Sladen and Hébert 2008).

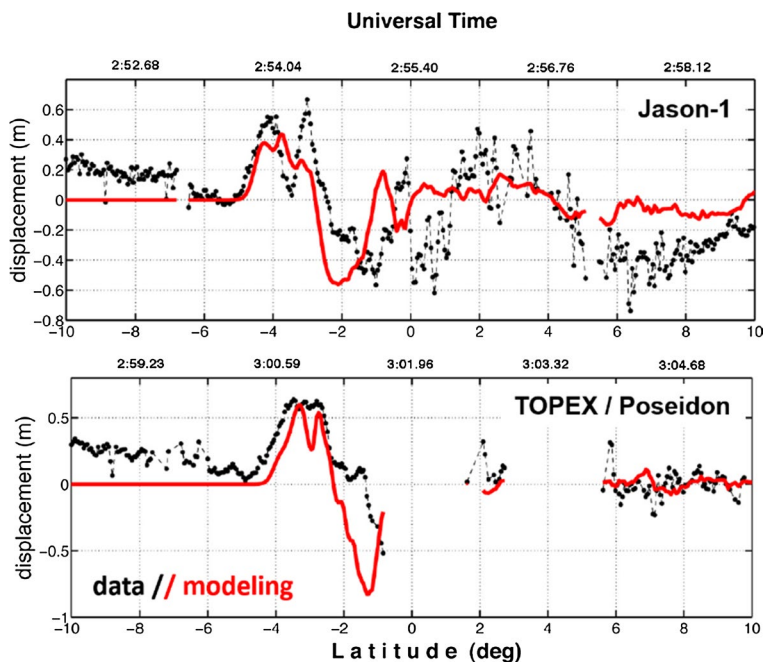


Fig. 7 Altimetry signatures of the 2004 Sumatra tsunami, with measurements of the ocean surface (black) for the Jason-1 (top) and Topex/Poseidon (bottom). The synthetic ocean displacements are shown in red (Figure from Occhipinti et al. 2006)

This observation still remains exceptional, and the 2011 tsunami could not be recorded at such an early stage of the propagation, not necessarily because of smaller amplitudes, but due to satellite tracks not properly crossing the tsunami front waves in their temporal distribution. The available maximal amplitudes, from 20 to 60 cm, were available on Envisat, Jason 1 and Jason 2, from 5:20 to 8:25 h after the earthquake (Song et al. 2012), and were not as useful as in 2004 to retrieve any information on the source processes.

It should also be kept in mind that the altimetry profiles give a picture of the tsunami propagation along tracks, crossing the area by chance. Even though almost static compared to the tsunami propagation time scale, they do not provide full insight into the accurate description of the waveforms. The full temporal description of amplitudes and phases are usually more efficiently recovered through measurements using sea-level sensors, though only located at specific fixed locations.

4.3 Atmospheric Gravity Waves

Tsunamis can trigger acoustic and gravity waves that propagate upward into the atmosphere. Infrasound waves were detected following the 2004 tsunami, thanks to infrasound measurements made by the International Monitoring System (Comprehensive Nuclear-Test-Ban Treaty) (Blanc et al. 2018; Marty 2019). They were associated with the possible coastal impact in the Bay of Bengal, during the shoaling phenomenon (Le Pichon et al. 2005).

Gravity waves of lower frequency are also observed at ground level thanks to infrasound networks (e.g., Hupe et al. 2019). In space, those induced by tsunami waves triggered by the 2011 Tohoku earthquakes were reportedly detected thanks to GOCE (Gravity Field and Steady-State Ocean Circulation Explorer) accelerometer data (Garcia et al. 2014). High-frequency perturbations of the associated parameters were observed during three crossings of the tsunami waves by the GOCE trajectory. These rare signals could be explained consistently with a gravity wave model and also provided the propagation azimuth of the gravity waves. Other missions dedicated to the measurement of the variations of Earth's gravity field such as GRACE (Gravity Recovery And Climate Experiment) could also theoretically produce signals related to the coupling of tsunami waves upwards in the atmosphere.

4.4 Total Electron Content in the Ionosphere from GNSS and Altimetry

An outstanding capacity for measuring tsunamis coupled in the atmosphere now relies on GNSS data. Permanent GNSS networks dedicated to tectonic observations and real-time precise positioning are able to measure ionospheric Total Electron Content (TEC) variations (Mannucci et al. 1998; Lognonné et al. 2006) induced by a tsunami (Fig. 4). The TEC represents the ionospheric electron density integrated along the ray-path between ground-based or space-borne receivers and satellites. Precise GNSS positioning makes use of two radio frequencies (1.2 and 1.5 GHz) to correct for the dispersive delay induced by the ionospheric plasma on radio signals, thus providing TEC measurement. As the density of the ionospheric plasma is strongly peaked, the TEC measurements are usually considered to be located at the altitude of maximum electron density, that is, at around 300 km altitude.

Ionospheric seismology (Lognonné 2009; Jin et al. 2015; Occhipinti 2015; Jin 2019; Astafyeva 2019), in essence the branch of seismology studying the effect of earthquakes and tsunamis in the atmosphere and detectable in the ionosphere, took great advantage of the measurement of the TEC by GNSS. A first detection of tsunami propagation, and

subsequent coastal impact when reaching Japan about 22 h after the generation, was achieved after the tsunami following the 2001 Peru earthquake ($M_w = 8.1$), thanks to the dense Japanese GPS network GEONET (Artru et al. 2005).

Today dense GNSS arrays in Japan (GEONET network), USA (PBO network) or New Zealand (GEONET NZ network) allow the imaging of the ionosphere finely and widely (Fig. 8). These measurements have been completed by satellite to satellite occultations, such as using the COSMIC system, which have been able also to detect tsunami ionospheric signals, but with very different sounding geometries (Coisson et al. 2015, Yan et al. 2018).

In the near field, the detection of acoustic-gravity waves coupled with the uplift at the source (AGW_{epi}) by GNSS-TEC permits the imaging of the source extent about 8 min after the rupture (Astafyeva et al. 2011, 2013, 2019) (Fig. 4). It visualizes the source propagation pattern of the AGW_{epi} , and also in the far field the Rayleigh waves (AGW_{Rayleigh}) and the tsunami (IGW_{tsuna}) signatures in the ionosphere (Artru et al. 2005; Occhipinti et al. 2013), including the oceanic region overlooking the rupture not covered by any other sensors, or rarely by GNSS buoys giving local measurements only.

In the same way as GNSS, altimetry data also make it possible to estimate the total electron content. Indeed, the TEC is required to remove the ionospheric effects from the altimetric data (Bilitza and Rawer 1996) for reliable measurements.

In the case of the 2004 Sumatra tsunami, the Topex/Poseidon and Jason-1 satellites showed the tsunami signature at the same time on the sea surface (Fig. 7) and in the ionosphere (Fig. 9). Using a three-dimensional numerical modelling (based on the linearized momentum and continuity equations, for irrotational, inviscid and incompressible flow), Occhipinti et al. (2006) created a pseudo-spectral propagator to transfer the oceanic displacement (from a tsunami model) to the atmosphere/ionosphere to compute the IGW_{tsuna} generated by the Sumatra tsunami. This quantitative approach reproduced the TEC observed by Topex/Poseidon and Jason-1 over the Indian Ocean on 26 December 2004, thereby validating the detectability of tsunamis by ionospheric sounding.

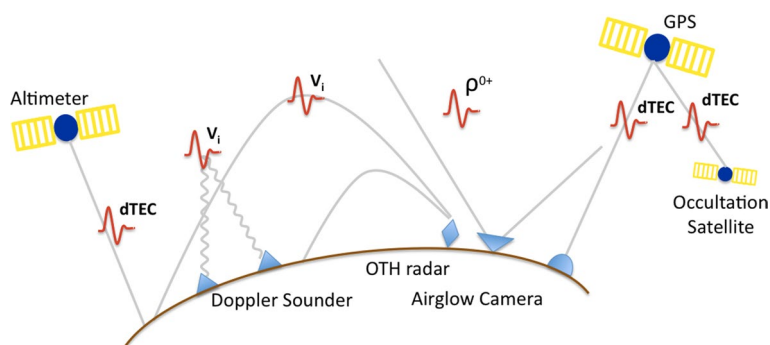


Fig. 8 The interaction of the AGW_{epi} , IGW_{tsuna} and AW_{Rayleigh} with the ionosphere produces strong variations in the plasma velocity and plasma density observable by ionospheric sounding techniques. Nominally, the altimeters and GNSS measuring the total electron content (TEC) (expressed in TEC units (TECU); $1 \text{ TECU} = 10^{16} \text{ e}^-/\text{m}^2$); the Doppler sounders and Over-The-Horizon (OTH) radars measuring the vertical displacement of the reflection layer in the ionosphere; and the airglow camera at 630 nm measuring a photon produced by the recombination of the oxygen, at 250 km of altitude, and directly related to the O^+ density. (Figure from Occhipinti 2015)

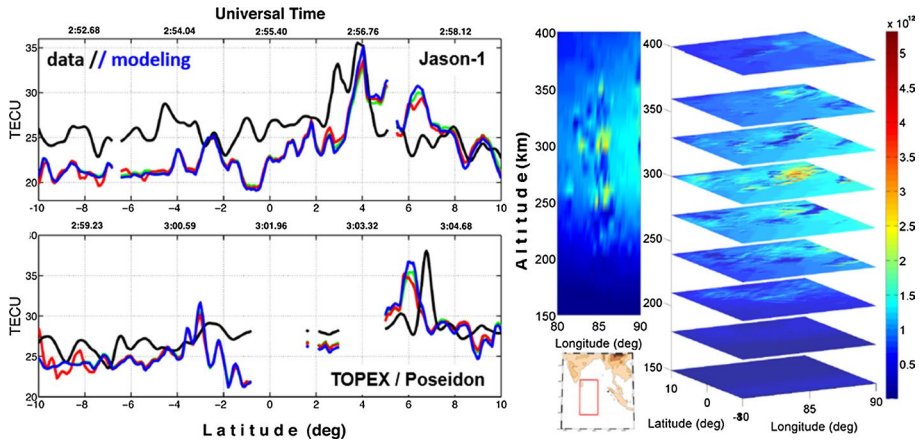


Fig. 9 Sumatra earthquake, 2004; the modelled and observed TEC are shown for Jason-1 and Topex/Poseidon satellites: data (black), synthetic TEC without production-recombination-diffusion effects (blue), with production-recombination (red), and production-recombination-diffusion (green). Right: electron density perturbation produced in the ionosphere by the tsunami gravity wave to model the TEC perturbation (vertical integration of the electron density along the line of sight) (From Occhipinti et al. 2006)

The results were later reproduced by Mai and Kiang (2009), and other theoretical works followed Occhipinti et al. (2006) to calculate the effects of dissipation, viscosity and thermal conduction on the IGW_{tsuna} (Hickey et al. 2009). More recently, electromagnetic field perturbations were accounted for in addition to viscosity and compressibility (Kherani et al. 2012); when complemented with a tsunami normal mode model (Coïsson et al. 2015), it provides a full direct coupling method from the ocean up to the TEC signal which proved successful in modelling (Rakoto et al. 2017). Although this kind of model uses a flat bathymetry, the agreement between synthetic and observed waveforms (DART and GNSS-TEC) was very satisfactory for several recent tsunamis (Kuril 2006; Haida Gwaii 2012; Tohoku 2011), at least for the first arrivals.

Rolland et al. (2010) generalized the ionospheric detection of IGW_{tsuna} for moderate tsunami events (Kuril, 2006, $M=8.3$; Samoa, 2009, $M=8.1$; Chile, 2010, $M=8.8$), analysing the GNSS-TEC observed by 50 receivers in Hawaii during the far-field tsunami propagation. They were able to reduce the empirical detection threshold to 2 cm, a figure similar to the height of the Samoa tsunami offshore Hawaii. Comparison between the GNSS-TEC observations and the oceanic DART data showed similarities in the waveform as well as in the spectral signature of the ionospheric and oceanic data. This result showed again that the ionosphere is a sensitive medium for detecting tsunami propagation. The study was confirmed by Galvan et al. (2011), while Grawe and Makela (2015) later highlighted the combined effects of the geomagnetic field and GNSS-TEC observation geometry in the cases of the 2011 Tohoku-Oki tsunami and the 2012 Haida Gwaii tsunami (induced by an $M=7.7$ earthquake). Similar results using the Hawaiian GNSS network have been obtained by Savastano et al. (2017) in a real-time scenario, basically using only the real-time information available from GPS receivers and satellites. The signature of the Tohoku tsunami (IGW_{tsuna}) in the TEC has been also detected using COSMIC radio-occultation (Coïsson et al. 2015), showing the possibility of additionally enlarging the coverage.

The catastrophic tsunamigenic earthquake in Tohoku, Japan, in 2011, reaffirmed the potential advantage of the GNSS-TEC ionospheric sounding to visualize tsunami

Fig. 10 GNSS-TEC observed during the 2011 Tohoku event by GEONET. From top left: at the earthquake time; at the first arrival in the ionosphere of the AGW_{epi} after 8 min, and 1 min later; 27 min after the event the signature of the AW_{Rayleigh} is observed and, last column, 56 min after the event, there is clear evidence of the IGW_{tsuna} . Adapted from a video related to Rolland et al. (2011)

generation and tsunami propagation (Rolland et al. 2011) (Fig. 10). The GNSS-TEC observation of the IGW_{tsuna} in the far-field has been also successfully inverted by Rakoto et al. (2018) to estimate the oceanic displacement with a resolution comparable to that of the DART buoys. The capability to reproduce the tsunami signature in the ionosphere (IGW_{tsuna}) is now demonstrated by several modelling approaches: for example, Rakoto et al. (2017) used a 1D model, integrating atmosphere variability and normal mode summation (Lognonné et al. 1998). Other techniques have been developed, with full wave modelling (Hickey et al. 2009, 2010a, b; Yu et al. 2017), with wave perturbations of Global Ionosphere-Thermosphere models (Meng et al. 2015, 2018) or with vertical spectral or time upward propagation (Broutman et al. 2014; Huba et al. 2015; Vadas et al. 2015), among others.

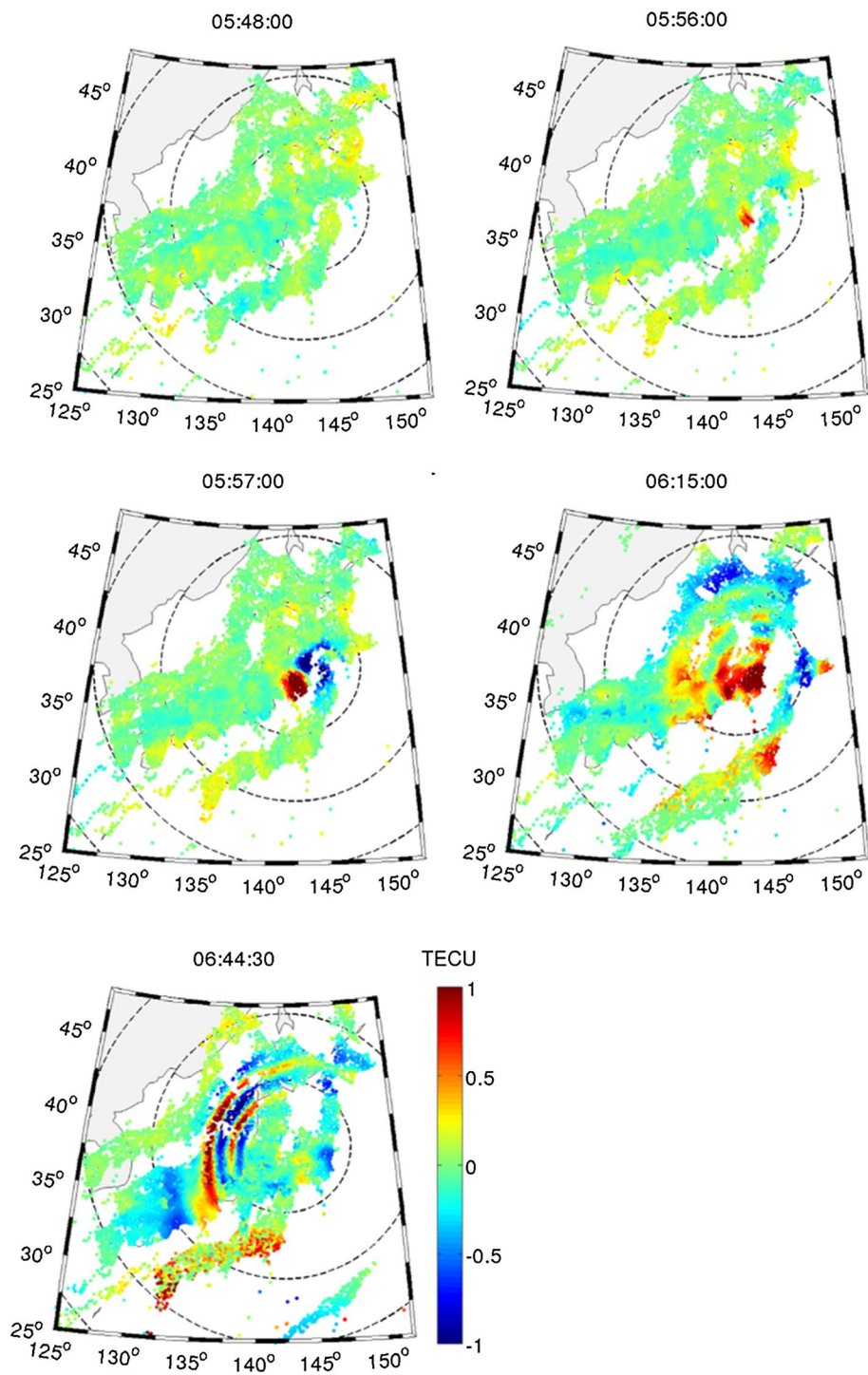
The estimation of the oceanic displacement by GNSS-TEC observed during the Tohoku earthquake has also been generalized to several events (Rakoto et al. 2018), who demonstrated the capability of such modelling to estimate ocean height estimation to $\sim 10\%$ of a posteriori errors. However, these approaches have to be generalized for all kinds of tsunami heights and wavelengths.

4.5 Airglow Signal

Although not based on satellite platforms so far, additional works theoretically explored the detection capability of IGW_{tsuna} by a ground-based airglow camera (Hickey et al. 2010b) and over-the-horizon radar (Coisson et al. 2011). During the Tohoku tsunami, in addition to TEC-GNSS measurements, the 630 nm airglow camera located in Hawaii, observing the O^+ night density variation, showed, for the first time, the internal gravity waves forced by the tsunami (IGW_{tsuna}) in a zone of $180 \times 180 \text{ km}^2$ around the island (Fig. 11). This method showed the observation of the tsunami ionospheric signature with an unprecedented high spatial density, visualizing the tsunami propagation across a wide area, rather than using local buoy measurements (Makela et al. 2011; Occhipinti et al. 2011).

The tsunami signature was successfully identified thanks to the matching of the waveform reproduced by numerical modelling (Occhipinti et al. 2011), a fact that also highlights the role of the bathymetry: approaching the Hawaiian archipelago, the tsunami propagation is slowed down (due to the reduction of the sea depth), but the IGW_{tsuna} , already formed and propagating in the atmosphere/ionosphere conserves its speed and arrives before the tsunami wave-front, slowing down near the shore (white-dotted-lines, Fig. 11). The Tohoku tsunami has maximum energy at two main periods of 14 min and 26 min, with the longer period wave propagating faster (Occhipinti et al. 2011).

A visual 2D cross-correlation between the observation and modelling highlights a shift of around 2° in both directions, potentially explained by the effect of the wind (which is not included in the modelling), as anticipated by Occhipinti et al. (2006). The airglow camera in Hawaii was unfortunately not calibrated, consequently, the comparison between data and synthetic results is only qualitative (based on the shape of waveform and arrival time) and does not allow the explicit connection between the observed number of photons and the amplitude of the tsunami. The tsunami signature



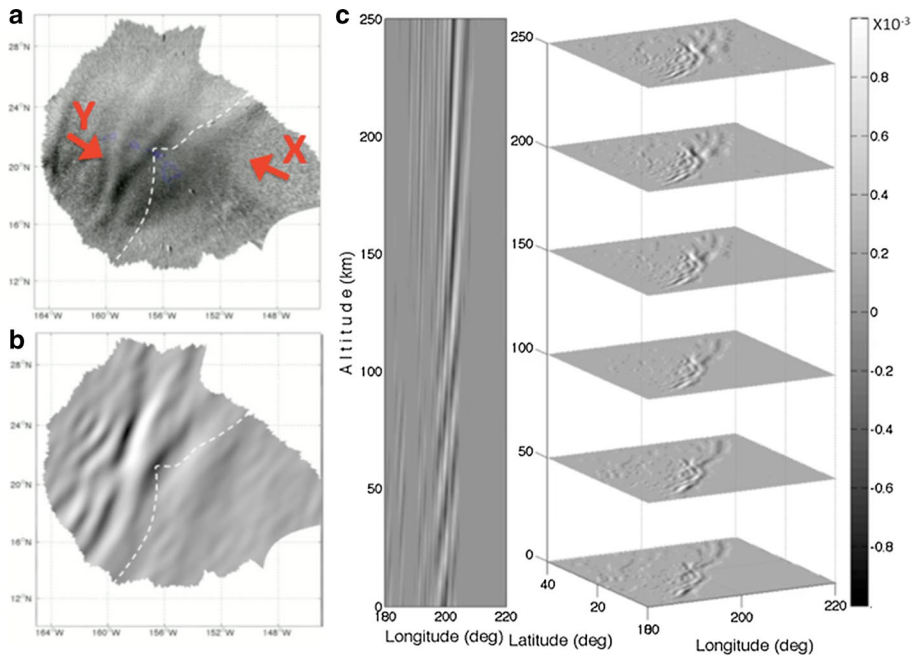


Fig. 11 Tohoku tsunami (2011) IGW_{tsuna} observed by the 630 nm airglow camera in Hawaii (a), modelled at the layer of observation (250 km) (b), and full 3D (c). Dotted-white-line shows tsunami wave-front, Y and X the IGW_{tsuna} at periods of 14 min and 26 min, respectively (red arrows highlight the position, not the direction) (Figure from Occhipinti et al. 2011)

in the O^+ density was also successfully detected by the calibrated 630 nm airglow camera located in Argentina, 18,000 km away from the epicenter (Smith et al. 2015), confirming again the potential interest and reliability of the optical tsunami detection by ground-based airglow cameras.

Two additional tsunami events have been successfully detected by the airglow cameras in Hawaii: the moderate Queen Charlotte Island, Haida Gwaii, earthquake ($M=7.7$, 28 October 2012, British Colombia) which created only a couple of centimetres of tsunami wave amplitude and no damage, and was detected despite the unpropitious observation conditions (quasi-full moon whose light reduces the sensitivity of the airglow camera) (Grawe and Makela 2015); and secondly the tsunamigenic earthquake in Illapel, Chile ($M=8.3$, 16 September 2015, few fatalities and several areas of damage) (Grawe and Makela 2017). In any case, $AW_{Rayleigh}$ are routinely detected by Doppler sounders (Artru et al. 2004) and OTH-radar (Occhipinti et al. 2010) for events with a magnitude larger than 6.5. Occhipinti et al. (2018) introduced the ionospheric magnitude showing that ionospheric monitoring is a valuable and trustworthy method of seismological observation sensitive to the source parameters. Nevertheless, the experimental airglow camera deployed in Pamatari in Tahiti from 2016 to 2017 was unable to record any relevant tsunami signal (Reymond, personal communication), because there were no significant tsunamis during that observing period. It also serves as a reminder that such instruments detect only under specific conditions that must be guaranteed (dark nights and obviously without contamination by, e.g., nearby forest trees).

The first satellite-based observations of tsunami-induced airglows (Yang et al. 2017) therefore create the potential for future space-based observation to be able to obtain better continuity of the ionospheric monitoring from above the Earth.

4.6 Global Navigation Satellite System Reflectometry (GNSS-R)

Finally, GNSS-R is an innovative way of using GNSS signals for remote sensing. It uses ocean reflected GNSS signals for sea surface altimetry. But, in contrast to conventional satellite radar altimetry, multiple height measurements within a wide field of view can be made simultaneously.

Two GNSS-R altimetry approaches, the code altimetry and the carrier phase altimetry, can be distinguished from each other. In the code altimetry or PASSive Reflectometry and Interferometry System (PARIS) concept proposed by Martin-Neira (1993), the time delays between the direct and reflected signals are measured, which can be translated into the absolute height of the reflecting surface at the specular point. In ground-based GNSS reflection experiments above an artificial pond, height accuracies of 1 cm can be obtained (Martin-Neira et al. 2002). In a series of airplane and balloon experiments, this technique was successfully applied in airborne campaigns (Rius et al. 2002; Ruffini et al. 2004). In these experiments, sea-level heights with accuracies of up to 5 cm, as well as the relation between C/A-code correlation function and significant wave heights, were determined using dedicated delay mapping GPS receivers.

It was then proposed (Stosius et al. 2010) that strong tsunamis induced by earthquakes of magnitude $M > 8.5$ could be detected with certainty from any orbit altitude within 15–25 min by a 48/8 or 81/9 Walker constellation (Walker 1984), given the idea that tsunami waves of 20 cm or more can be detected by space-borne GNSS-R.

If the three GNSS networks (GPS, GLONASS and Galileo) are combined, a better detection performance can be expected for all scenarios considered (Stosius et al. 2011). In this case, an 18-satellite constellation would have detected the 2004 Sumatra tsunami within 17 min with certainty, while it takes 53 min if only GPS is considered, showing the growing interest in utilizing multiple GNSS systems. With a dedicated Low Earth Orbit (LEO) constellation of satellites equipped with GNSS-R receivers, densely spaced sea surface height measurements could be established to detect tsunamis in the future. Recovering accurate tsunami heights from such a technique remains, however, uncertain.

4.7 Conclusions on the Various Techniques Available to Measure Tsunamis

In the earlier sections, we have shown how the usual ways of characterizing possible tsunami sources and propagation were significantly improved thanks to major improvements appearing from the satellite data. Previously based on a limited number of tide gauges deployed in harbours, the tsunami waveforms are now also made available during the propagation, not only from pressure gauges deployed since the 1990s on the sea-floor (DART buoys), but also on GNSS buoys anchored closer to the shore. Space missions, not based on ground sensors, such as altimetry, have provided limited insight into tsunami propagation so far. By contrast, GNSS data relying on ground sensors brought a striking improvement to indirectly accessed tsunami characteristics obtained through TEC measurements.

5 Coastal Effects of a Tsunami and Improved Risk Prevention

Measurements of sea-level variations that offer a quantitative view of the tsunami wave-forms at several coastal locations are very useful to tsunami scientists, as seismograms are essential to seismologists. But civil protection and emergency services rapidly need, through interpreted data, an assessment of the areas that have been affected by the tsunami waves, to quantify the structural and human damage over the flooded area. Satellite imagery thus gives additional constraints on the flooding extent, the damage intensity and the coastal vulnerability (Borrero et al. 2006; Chen et al. 2006). International cooperation is efficient in case of catastrophic disasters, in order to open data useful for the damage detection and to help the crisis management. This effort is effective since 2000 by the International Charter Space and Major Disasters composed of space agencies and space system operators all over the world (Bessis et al. 2004).

5.1 Damage Assessment Through Optical Imagery

One example of the contribution of satellite imagery to post-tsunami studies was crucial in the aftermath of the 2004 disaster, particularly in Indonesia's Aceh Province. Indeed, at the time, this province was one of the most isolated in Southeast Asia because it was in the grip of a civil war between the Indonesian Army and separatist forces. As the province was closed to foreigners and journalists, the damage caused by the tsunami was initially assessed by satellite imagery, in addition to an unprecedented amount of video footage and pictures.

Several images were quickly posted on the internet, including a 60-cm resolution Quickbird image produced by Digital Globe on 28 December 2004, 2 days after the tsunami. This was compared with the previous one dated 23 June 2004 (Fig. 12, a and b). In the weeks and months following the disaster, field studies organized as part of the various field trips coordinated by UNESCO (International Tsunami Survey Team-ITST) or specific research programs such as TSUNARISK (Lavigne et al. 2009) gave the opportunity to refine the first observations from aerial imagery and to provide more precise data of altimetry, wave height and run-up. Figure 12a, b shows the damage in the harbour area of Ulee Lheue, northwest of Banda Aceh, resulting from the combined action of subsidence caused by the coseismic vertical deformation, and by erosion caused by the tsunami. In this area, the subsidence reached an amplitude of about 1–1.5 m, which partly explains the retreat of the coastline and the flooding of the fish ponds (tambak) which had gradually replaced the mangrove.

The comparative study of these satellite images also offers researchers to study the damage to buildings. In a 7 km² area between the Ulee Lheue harbour and downtown Banda Aceh, Leone et al. (2010) conducted a systematic diagnosis of the state of the buildings approximately 1 year after the tsunami. Their method of damage spatial analysis was based on a combination of field surveys, photo interpretations and GIS. They built a new “macro-tsunami” intensity scale based on a typology of building types and damage done.

Beyond the short-term impacts of tsunamis, satellite imagery also gives us the ability to study longer-term resilience, whether environmental or societal (i.e. reconstruction dynamics). Thus, 12 years after the 2004 tsunami, a shoreline mapping was reconstructed from an IKONOS image of 10 January 2017 at 1.5 m resolution and compared to previous ones. Figure 12c shows that the barrier island north of the port of Ulee Lheue has been almost abandoned.

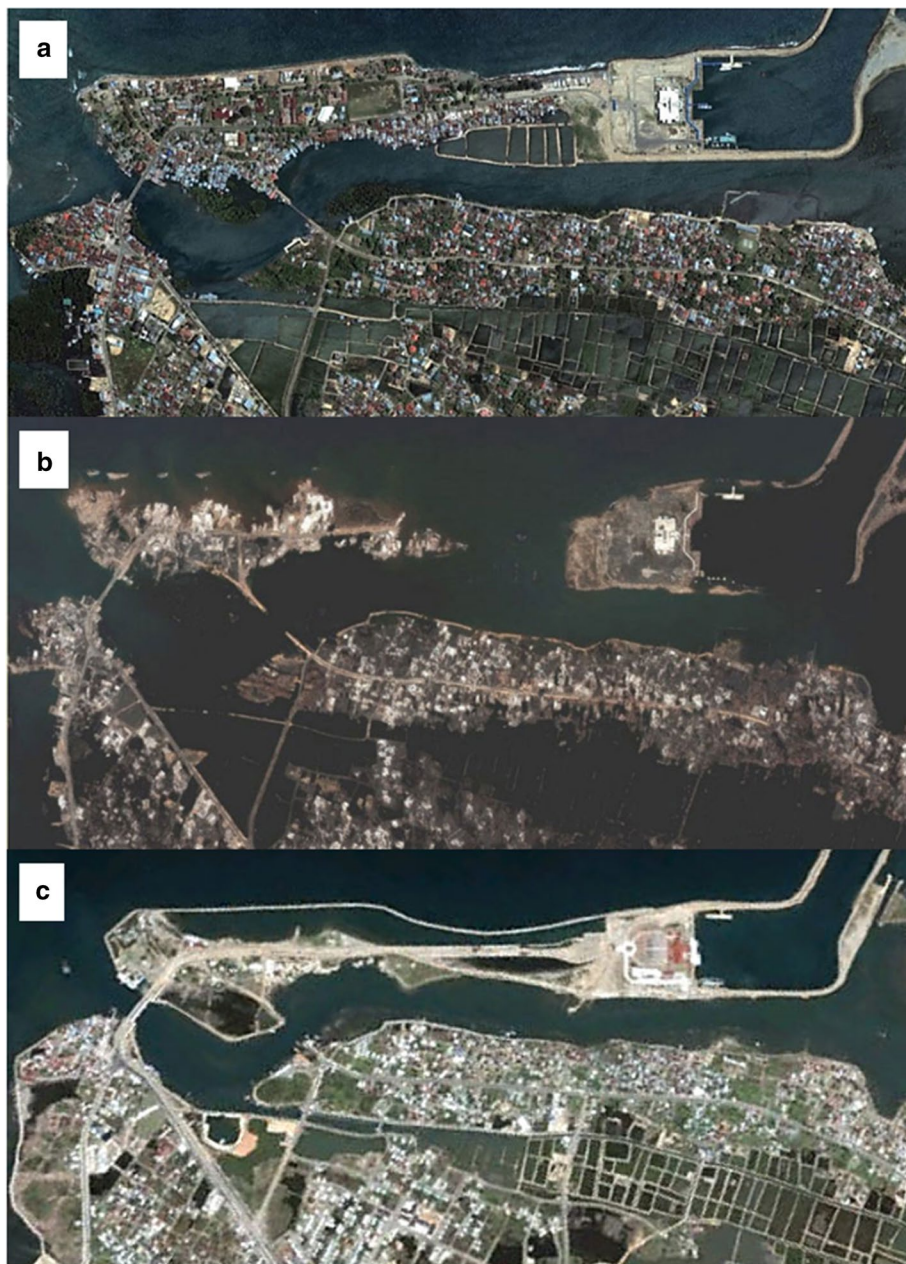


Fig. 12 Landscape modifications at Ulee Lheue harbour region, north western Banda Aceh. **a** Six months before the tsunami impact (Image Digital Globe on 23 June 2004, 60 cm resolution). **b** Two days after the tsunami impact (Image Digital Globe 60 cm resolution). **c** IKONOS image on 10 January 2017 (resolution: 1.5 m)

However, the area behind it has been completely rebuilt. Further west of the port, in the Lambadeuk district, large areas submerged by the tsunami have remained flooded to this day (Fig. 13a). In contrast, in the Kuala Gigieng area east of Banda Aceh (Fig. 13b), the shoreline has gradually returned to its original location, as subsidence may have been lower (around 60 cm), but mainly due to a significant volume of sediment deposited by the Aceh River.

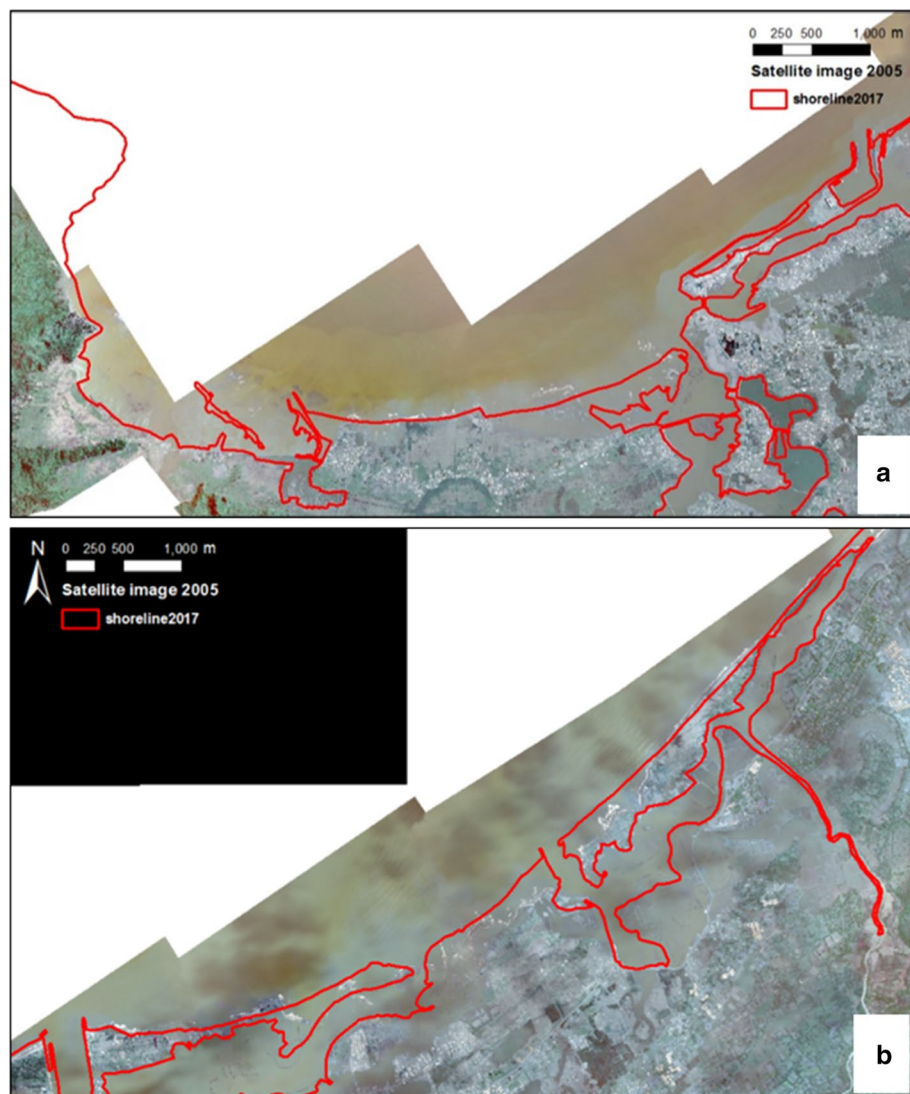


Fig. 13 Shoreline changes at the Banda Aceh coast between 2005 and 2017 (Meilianda et al. 2019). **a** Lambadeuk area, west of Banda Aceh, was more affected by the subsidence and has definitely lost several hectares of land. **b** Kuala Gigieng area, east of Banda Aceh, has now two relatively permanently open inlets, partly due to post-tsunami coastal aggradation

Satellite imagery is also of great help when mapping is required in remote areas where in situ measurements are not easily available. For instance, after the 2006 Java earthquake and tsunami (a so-called tsunami earthquake, provoking a tsunami much larger than the magnitude level could indicate, generally with a very slow seismic rupture, as defined in Kanamori 1972), the sector with suspected maximum run up values, reaching locally up to 20 m, was expected in an area with restricted access. Thanks to satellite imagery, the horizontal mapping of the inland flooding could be defined (Hébert et al. 2012). Run-up values which can then be estimated from the vertical heights only are available, which was in that case possible via a stereographic approach such as the one used to define DEMs.

5.2 Damage Assessment Through SAR Imagery

SAR imagery is obtained by the measurement of the backscattering of an electromagnetic wave emitted by a satellite. One of the main advantages of SAR compared to optical imagery is its all-weather capacity, i.e., images of the ground surface can be acquired even in cloudy conditions. SAR imagery is widely used for tsunami-related damage detection, using different approaches. For example, simple coloured RGB (red–green–blue) compositions can be produced with images acquired, respectively, before and after the event, in order to obtain a quick assessment of flooded or damaged areas. Such maps do not indicate any automatic classification of damaged or flooded pixels; nonetheless, they are very useful for civil protection purposes as their interpretation is simple.

More complex techniques permit the automatic detection of flooded (Iyyappan et al. 2018) and damaged areas, or even the automatic classification of the level of damage due to a tsunami. Some authors use SVM (Support Vector Machine) classification schemes (Endo et al. 2018), sometimes applied to polarimetric SAR data which gives valuable information on urban areas (Ji et al. 2018). Indeed, as polarimetry brings information on different backscattering mechanisms, it is possible to characterize the condition of buildings. Recently, some studies have been aimed at rapid damage assessment using Deep Neural Networks on SAR images (Bai et al. 2018) or data fusion between optical and SAR data (Adriano et al. 2019). These assessments could then be used for civil protection.

Below we show a simple example of a coloured composition on the 2011 Tohoku great tsunami. The German satellite TerraSAR-X, which operates in X-band (about 9 GHz), acquired images over the Sendai region before and after the tsunami. Figure 14 shows the RGB composition of two images acquired on 20 October 2010 and 12 March 2011. The first image is in the blue and green channels (or equivalently a cyan channel). The second image is in the red channel. The areas where no change occurred between the two dates appear in grey levels, from black (for low backscatter pixels) to white (for high backscatter pixels). The pixels where backscattering is higher (respectively lower) on the first date than on the second one, appear in cyan (respectively in red), thus highlighting a change.

Land areas appearing in cyan are flooded areas. Indeed, as can be seen on the upper inset, the backscattering of the radar wave on water is very low: since it is lower than the backscattering of land, flooded areas appear in cyan. These areas can very easily be detected from this map: it can be observed that very large areas have been flooded, in particular between the shoreline and Sendai city. On the sea, the cyan structures on the upper inset correspond to shellfish farming that was destroyed during the tsunami. Red pixels correspond to debris with high backscattering, coming from shellfish farming (along the shoreline on the upper inset) or other debris (as on the airport area).

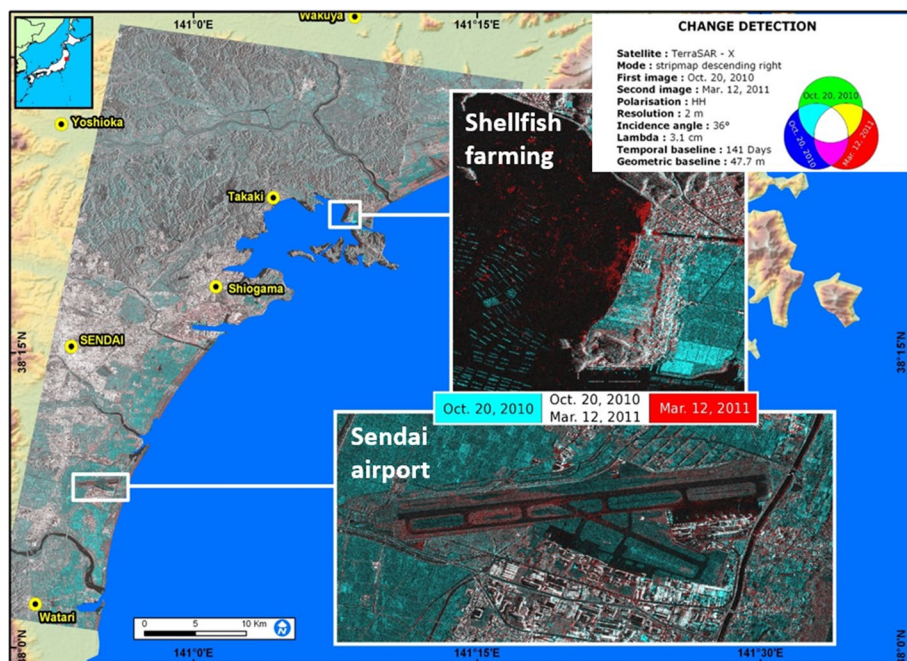


Fig. 14 Change detection obtained from TerraSAR-X images acquired on 20 October 2010 and 12 March 2011, showing the impact of the 2011 Tohoku tsunami in the area of the Sendai plain. The upper inset shows destroyed shellfish farms while the lower inset shows debris on the Sendai airport

Such SAR analyses are usually carried out after the events, to estimate damage in addition to ground deformation. The need for an available image prior to the event, and for real-time processing, makes this technique still poorly available in real time.

5.3 Towards Improved Risk Prevention and Resilience Capacity

Tsunami data acquired following disasters helps local risk prevention plans to be established for the benefit of the coastal communities threatened by such events. Space data, and especially GNSS positioning, have continuously improved the technologies used to draw maps with the required accuracy and resolution. Combined with hazard maps deduced from appropriate numerical modelling, the tsunami risk maps now integrate many products and types of information derived from satellite data. The same applies for the design of evacuation routes and assembly areas. Such crucial maps can also be continuously updated through the use of optical and radar imagery that monitors major changes in land use.

As satellite data play a growing role in understanding the processes and helping to create better preparedness for tsunami damage, it is easy to understand that it now deeply integrates the various stages involved in a tsunami warning system.

6 Which Space Data are Required for Tsunami Warning Systems (TWSs)?

In this section, we propose to investigate which satellite mission could be useful in the frame of tsunami real-time warning. To this end, data from such space missions should not only be available in real time and over all the areas exposed to tsunamis, but their processing or analysis should also be made available to decision makers very rapidly. Consequently among the techniques exposed previously, it is highly improbable that InSAR, sea-level measurement by altimetry or GNSS-R techniques may be useful in the first minutes. Conversely, tsunami scientists are more and more interested in data derived from GNSS techniques, whatever for sea-level measurements on buoys, or TEC measurements, or for the quick description of surface ground deformation that allows for source inversion. These data will play a growing role in tsunami warning, which however still essentially relies on seismology and satellite robust communication.

6.1 Principle of TWSs and the Situation After 2004

The essence of a tsunami warning system (TWS) is the prompt detection of the geophysical event prior to possibly triggered tsunami waves, combined with the measurement and monitoring of sea wave heights throughout the oceanic basin where they would propagate. Due to the time scales of a tsunami, such monitoring can last for hours; however, the role of the TWS is crucial in the first few minutes following the initiation, in order to warn the authorities.

Early detection is more effective for an earthquake than for a landslide, since seismic networks are now very efficient at providing a quantitative estimation of the main parameters of the mainshock. For a landslide, however, it still remains a challenge to have the equivalent characterization, unless very dense networks are available near every landslide-prone area.

Since the tsunami waves propagate more slowly than the seismic waves, the tsunami can then be monitored along its propagation in the minutes and hours following the earthquake, provided data can be acquired and transmitted. Originally relying on tide gauges deployed in harbours and locally transmitted through radio and progressively upward to satellites, the monitoring confirmed the occurrence of a tsunami and the ability to keep on updating warning status (while tsunami amplitude remained greater than 1 m). With the development of global seismic networks, a system such as the one designed in the Pacific Ocean back in the 1960s would have also been able to monitor the global seismicity and to give assistance for oceanic basins without an operational warning system. However, in the early 2000s, no global international architecture was established, and national initiatives did not exist to consider setting up tsunami warning systems. Thus, in 2004, there were no international procedures or contact points to receive and interpret the messages that the PTWC in Hawaii could send within the Indian Ocean.

Following the 2004 disaster, the Indian Tsunami Early Warning System (ITEWS), the set-up of which was started in 2005 (IOC 2005a), was completed by September 2007 (Nayak and Srinivas Kumar 2008a, b; Uma Devi et al. 2016). The ITEWS monitors seismically active regions of the Sumatra-Java subduction (4000 km long) and of the Makran coast (500 km) in the Arabian Sea (Gupta 2005, 2008). In addition to the essential

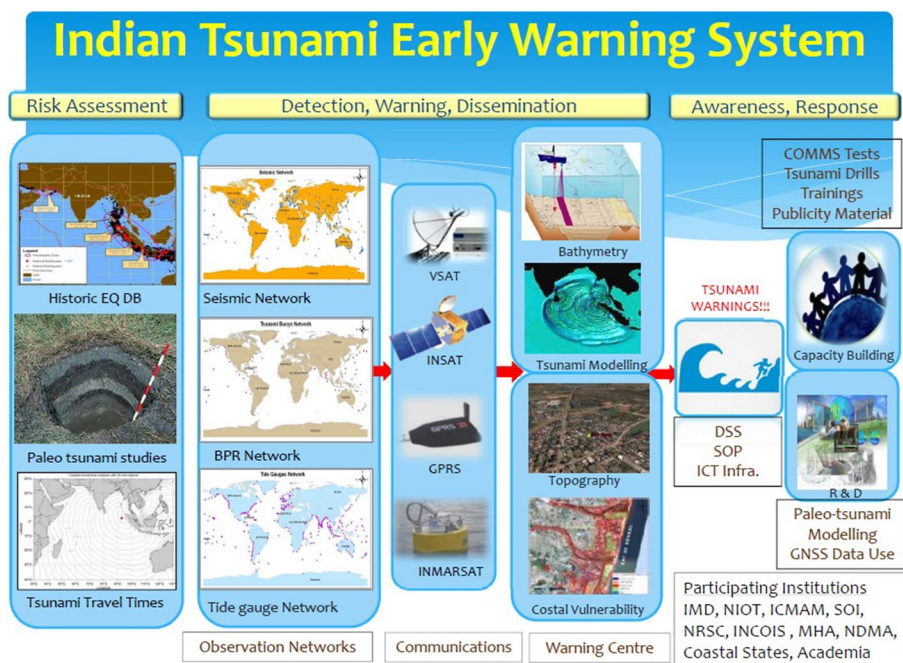


Fig. 15 Various components of the Indian Tsunami Early Warning System (ITEWS). Three approaches contribute to an efficient tsunami warning, a view shared among all TWS: the risk assessment, the operational detection and dissemination, and the high level of awareness and response capacity. Most of the components partly rely on space data or satellite means (courtesy, Indian National Center for Ocean Information and Services (INCOIS), Hyderabad, India)

components of a typical TWS mentioned above (Fig. 15), the ITEWS also includes ocean Bottom Pressure Recorders (BPRs) that encompass the two sources of tsunamigenic earthquakes.

The whole ITEWS makes use of Earth observations in multiple ways and illustrates well the three main pillars of an efficient system: hazard assessment, efficient warning procedures, and preparedness (Fig. 15). ITEWS has been working efficiently since 2007, complying with the IOC requirement of issuing any advisory within 10–15 min of time after an earthquake, in 8 min on average. False alarms are avoided, reminding us that before the establishment of the ITEWS, the 28 March 2005 Nias $M_w=8.7$ earthquake occurred in the vicinity of the 26 December 2004 Sumatra earthquake, and that a tsunami warning was issued by the Pacific Tsunami Warning Center (PTWC) and by the JMA (Japan Meteorological Agency). Consequently, millions of citizens living on the east coast of India were evacuated away from the shoreline, while this large earthquake did not trigger any large tsunami due to a particular low coupling with the ocean (Kerr 2005).

In the Caribbean and in the North-East Atlantic and Mediterranean (NEAM) regions, seismic networks and sea-level stations have been greatly developed since 2005, with a growing number of real-time data exchanges and capacity building of the national systems.

6.2 Seismological Challenge

Based on seismic detection, the early warning system has always been essentially seismological, and this remains the same up to the present time. In the first minutes after an earthquake, magnitude, depth and location are quickly available depending on the networks, but it is difficult to estimate the direction, duration, size (length and width) and exact location of the rupture (relative to the hypocenter). Yet these parameters are major influences of the tsunami triggering, and generally the complete seismological solutions start being stable after about 30 min.

In the first few minutes after the 26 December 2004 earthquake, its magnitude was estimated to be 8.5. This was an underestimate, due to the low frequency content of the seismic waves that was not properly taken into account in the numerical methods routinely used (Lay et al. 2005). Indeed such a magnitude had never been reached since the rise of modern seismic networks and since the last equivalent earthquakes in the 1960s in the Pacific Ocean. Again in 2011, in a well-prepared operational context, the first estimates routinely used in operation by JMA were able to produce a magnitude M_j of 7.9 only (based on broad band saturated seismic data), which was revised to 8.8 about 50 min later (JMA 2013).

Nevertheless it is necessary for some recent advances to be stressed, especially those which helped to reduce delays before obtaining focal mechanisms. For example, the low-frequency W seismic phase (Kanamori and Rivera 2008) helps to quickly provide the first estimations of the focal mechanism, which is a key information on the rupture pattern. A finer examination of the first minutes of the seismic signal influenced by the gravity changes also offers a rapid indication of the possible large magnitude in case of mega earthquakes (Vallée et al. 2017) prone to trigger tsunamis. Most of the TWS have adopted such rapid W phase techniques (see Duputel et al. 2011 for the Pacific Ocean; Roch et al. 2016 for NEAM region) that prove efficient in the near field. Warning systems watching more distant shorelines still follow methods adapted from long period surface wave inversions and are numerically made more efficient (Clément and Reymond 2015, for French Polynesia); although they are less rapid, they produce a robust and accurate focal mechanism.

In this early part of tsunami warning, it is essential to share, via satellite communication, seismic data, information and naturally to disseminate the first messages. Later on, when the tsunami propagates across the ocean, sea-level data again must be transmitted on the most robust basis.

6.3 Robust Communication for Scientific Data and Message Dissemination

The Global Telecommunication System (GTS) satellites (WMO 2018) are used by the tsunami warning systems for two purposes. First, the transmission of the tide gauge data measuring the tsunami waves on coastlines are sent through GTS. The sampling time is generally 1 or 2 min and the latency varies from 6 min to 1 h. Secondly, the Tsunami Service Providers (TSP) send the alert or threat messages, via GTS to the services and tsunami warning centres connected to GTS. The time delay is generally very short, less than 1–3 min. One of the recent requests is the possibility to add files to GTS messages, and this option would enhance the capacities of the TWS.

The GTS transmission is essential, especially when it may be the only available telecommunication in remote places where the local communication system is not robust enough.

On the other hand, places that could be impacted by earthquakes and where ground communication could be damaged, including due to the lack of an electrical power supply, need satellite transmission for alert messages and information on sea-level data.

6.4 Increasing Use of Dense GNSS Networks to Characterize the Tsunami Source

As previously mentioned, GNSS data are now almost unavoidable to characterize earthquake and measure ground deformation where dense enough networks are available, and then also to invert for the fault source pattern. Using such data under operational constraints remains generally challenging. Japan is one of the few examples where dense GNSS networks can rapidly produce insights into the coseismic ruptures. Chile (Barrientos et al. 2018) and New Zealand networks are also being improved for that purpose.

In Japan, the March 2011 earthquake and tsunami in Tohoku, Japan, have shown how relevant dense GNSS networks can be, to compute, within minutes, the extent and amplitude of the ground deformation (Ozawa et al. 2011; Song et al. 2012). GNSS networks complement seismological analysis in capturing the fault rupture extension and location, and its slip amount (Yamamoto et al. 2016; Ohta 2012; Ohta et al. 2018). More recently, Melgar and Hayes (2019) highlighted the capacities of GNSS data in characterizing large earthquakes before the end of the rupture process.

However, considering areas with rare seismicity, such as the Ligurian Sea or the North African margin, it is questionable whether existing networks could contribute. The potential detectability through GNSS sensors can be investigated to define elements to optimize a possible GNSS network geometry. Potential tsunami scenarios related are compiled here, based on the operational databases in place of the French TWS part of the NEAMTWS (Gailler et al. 2013).

The tsunami pre-computed scenarios, under a classical approach followed in a TWS (Titov et al. 2005), rely on state-of-the-art regional seismotectonics, consisting of unit faults 25 kilometres long and 20 kilometres wide (Fig. 16) that can be combined to achieve magnitudes beyond 6.9 (Gailler et al. 2013). A threshold of 10 cm vertically is considered to be the minimum value able to be detected in real time by a dense GNSS network; recent improvements in the technology probably will allow a lower value, though the vertical component remains the most difficult to resolve.

In the Ligurian Basin, faults localized on-land are mainly normal, with a few thrust faults into the French part. In the Tyrrhenian Sea, there is also a major region of normal faults and in the Ligurian Sea, faults are mainly thrust and strike-slip (Fig. 16, top). Some 20 events are identified for which the induced deformation (positive or negative) is higher than 10 cm. Along the coast, sectors capable of detecting events leading to more than 10 cm of deformation can be identified (areas of La Spezia, Aleria, Piombino in Italy and at the French Italian border, between Cannes and Imperia).

In Algeria, most of the faults localized on-land are strike-slip, with a few thrust faults on the West part of Jijel area (e.g., Kherroubi et al. 2009). Offshore, all the faults are thrust faults (Fig. 16, bottom). There is a maximum number of 21 events for which the induced deformation (positive or negative) is higher than 10 cm, and again these areas can be mapped, between Annaba and Chetaïbi, and for the area near Collo (Fig. 16).

Note also that including events with higher magnitudes generates detectable deformations inland, especially in thrust fault zones. In addition, some inland earthquakes can also marginally contribute to a tsunami trigger some tens of kilometres away from the shore; dense GNSS networks would help to rapidly quantify a possible coupling

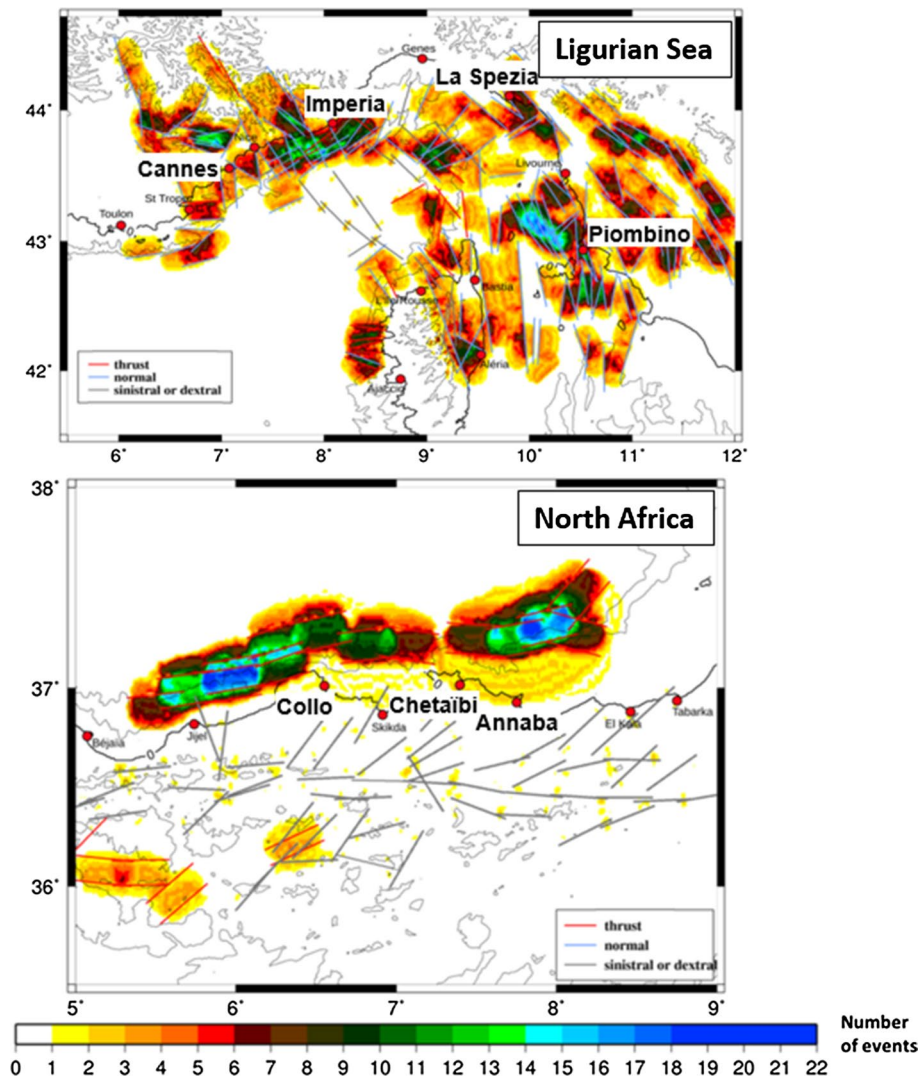


Fig. 16 Number of events mapped for the Ligurian Sea (top) and for Algeria (bottom), inducing a deformation higher than 10 cm (in absolute value) for magnitude up to 6.9 for Liguria, and to 7.5 for Algeria. Unit faults are 25 km long and 20 km, and the associated unit tsunami scenarios consider a 1 m slip. For the Ligurian Sea, 226 unit faults are considered and used as rupture zone triggering tsunamigenic earthquakes of magnitudes of 6.0, 6.3, 6.5, 6.7 and 6.9. For the North Algerian area, 142 unit faults are taken into account for the magnitudes of 6.5, 6.7, 6.9, 7.2 and 7.5. Some coupling of two, three or eight contiguous segments can be done on the offshore area in order to achieve magnitudes beyond 6.9 (Gailler et al. 2013), increasing the total number of scenarios to 462 along the Algerian margin. The tsunami simulation code is used to calculate the initial deformation for each scenario on the GEBCO grid (GEBCO 2014), at 30 s resolution

offshore. Having had a modern real-time dense GNSS network on the North African margin, the tsunami trigger following the 1980 El Asnam (Algeria) earthquake could have been estimated in a few minutes after the rupture (Roger et al. 2011). Together

with an accurate numerical forecast, it could have contributed to estimate the range of the expected impact in Spain (significant, but less than 50 cm in most harbours).

Although most of the tsunamigenic deformation occurs in submarine parts, it is reasonable to foresee that denser networks will be available in the future with lower detection thresholds, and could increasingly contribute to rapid imagery of a rupture extension following an earthquake in these regions. Areas described previously, with large tsunamis expected, such as Japan and New Zealand, are already very innovative in that respect.

6.5 Rapid Landslide Detection

As previously indicated, landslide detection should rely on a dense geophysical network close to any area exposed to possible failure. Significant achievement has been made, for instance in the area of the Stromboli volcano which was hit by tsunami waves following a rock avalanche triggered by the eruption of December 2002 (Tinti et al. 2005). The volcano was monitored through a seismic network, and a tilt and GNSS network originally deployed in the 1990s, which had been updated from 2003 on (Bonaccorso et al. 2009) and greatly contributed to real-time information for the Civil Protection Authorities (CPA) (Puglisi et al. 2005).

The available datasets were statistically interpreted into thresholds so as to define and send alert messages to decision makers (Carlà et al. 2016). Thanks to InSAR, time series processing and the availability of free SAR data with a 6- to 12-day revisit time offered by Sentinel-1, it would be possible to predict catastrophic slope failures (Carlà et al. 2019a).

However, in general, landslide characterization is achieved a few days after its occurrence. For example, satellite optical imagery offers a complementary view of the landslide volume induced, both in the case of a subaerial event, and when images are available a few days later. This was the case, for instance, for the 2017 cliff collapse in Greenland, when tsunami waves were generated and flooded a village nearby (Paris et al. 2019). In the case of essentially submarine collapses, as in Krakatau 2018 (Paris et al. 2020), only high-resolution differential bathymetric mapping could help, and this is very rarely available.

6.6 Altimetry

Future altimetry missions with swath acquisition (e.g., international project SWOT, Surface Water Ocean Topography) will have reduced instrumental noise (about 1 cm in amplitude) and will ensure acquisition on a larger area than along single profiles. In the case of a scenario in the Mediterranean Sea, a tsunami following a large earthquake in Algeria (magnitude 6.8) would produce a signal of about 5–10 cm offshore, while the mesoscale signal, though in different wavelengths, is about 5 times larger in amplitude (Fig. 17). Accurate signal processing may allow the recovery of the tsunami signal in such future missions that have repetition times of only a few days (or less, with a suitable constellation).

The perspective of using such future swath altimetry not restricted to acquisition along a single profile will increase the number of records made across the oceans when a tsunami occurs. This, however, remains limited to tracks crossing the tsunami waves by chance, and, unless a dedicated constellation of such satellites is developed, with or without geostationary platforms that are able to watch a larger basin, this very informative data is not ready to integrate a full operational chain delivering messages within a few minutes after the tsunami triggering.

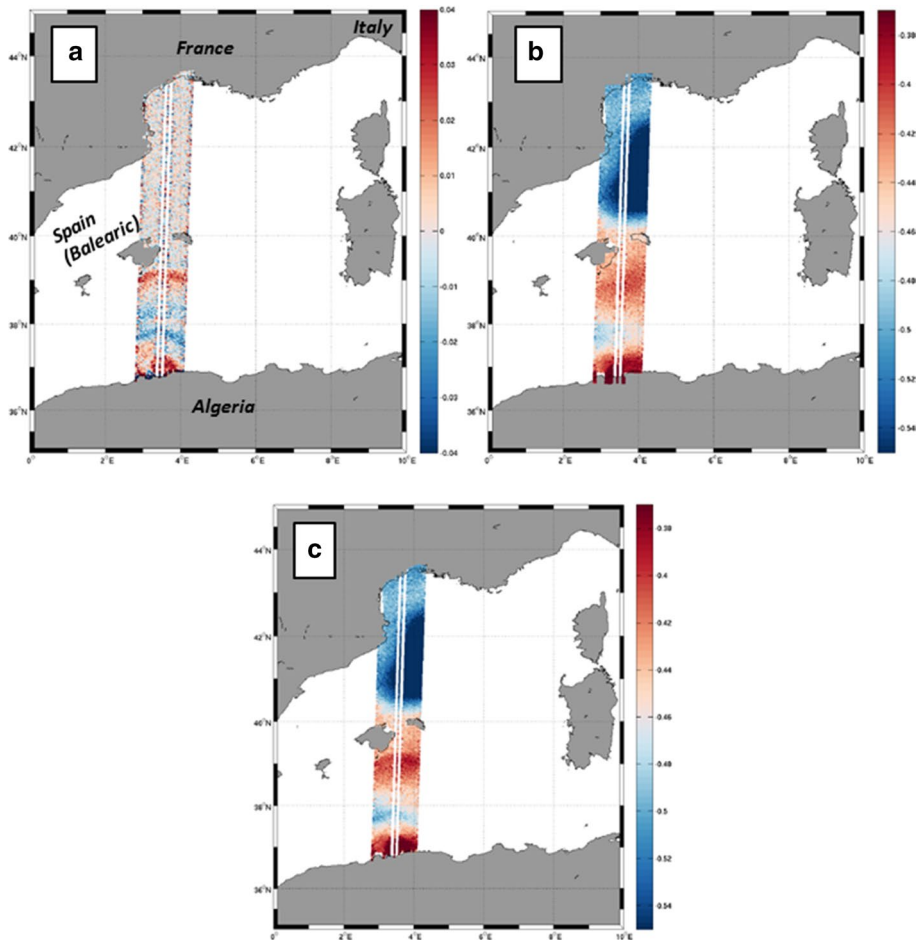


Fig. 17 Modelling of altimetry signals in the Western Mediterranean, in the case of a tsunami initiated in northern Algeria after a magnitude 6.8 earthquake (colour scale in metres). a) Model of the tsunami propagation with instrumental noise, b) model of the mesoscale dynamics showing larger wavelengths, and c) the sum of both contributions. The tsunami can be detected from the summed signal; its amplitude is about 20% smaller but with higher frequency content

6.7 Towards Real-Time Sea-Level Monitoring and Forecasting Using GNSS Buoys

Sea-level data available in real time throughout the warning is essential to monitor the propagation pattern during several hours, and it also integrates more and more numerical models on the fly, which in turn contributes to a better forecasting of remote tsunami impacts (Titov et al. 2005; Reymond et al. 2012; Clément and Reymond 2015; Jamelot and Reymond 2015). The offshore BPR (González et al. 2005), such as DART buoys, are very valuable as they can estimate the tsunami amplitude soon after their triggering by the earthquake. They are used to refine models and to compute real-time forecasts for specific sites.

This is, however, possible only when sea-level monitoring is available early to be incorporated, compared and/or assimilated (Yang et al. 2019) in the numerical approaches. In

that case, warning products gradually evolve to numerically-based forecast mapping, as in the USA (Titov 2009; Percival et al. 2018) or in French Polynesia (Jamelot and Reymond 2015).

Such sensors are now integrated in three out of four regional warning systems, but they require costly investment to maintain the devices in the long term. No such offshore tsunami sensor has been deployed in the NEAM region where land-based networks are not very dense on any of the surrounding coastlines, in particular along seismogenic zones.

The development of a dense network of GNSS buoys thus offers the possibility of delivering timely information on the sea-level status. On 11 March 2011, at 14:46 (local time), the Tohoku tsunami had its largest impact and run-up along the Sanriku coast. JMA, which is the authority in charge of issuing domestic tsunami warnings in Japan, was able to monitor sea-level changes at more than 170 tide gauges and 12 GPS buoys located about 20 km off the coast. The initial warning issued at 14:49 (local time) was based on the earthquake magnitude computed in JMA (Ozaki 2012), which proved to be underestimated because of the saturation of most Honshu broadband seismic sensors. Tsunami warning major upgrades issued at 15:14 and 15:30 (local time) were based on the tsunami wave observations at the GPS buoys.

After the experience of the 2011 event, JMA planned to improve its tsunami warning (Ozaki 2012), especially thanks to real-time algorithms such as Precise Point Positioning (PPP), the use of accelerometer data and with a network extending farther from the coastline. The implementation of an array of buoys deployed more than 100 km off the coast (Kato et al. 2018) would allow the rapid incorporation of sea-level data to refine the source model used for near-field tsunami forecasting systems (Tsushima et al. 2014). Such GNSS buoys could also contribute to multi-hazard monitoring, to study seafloor geodesy, atmospheric, and ionospheric disturbances with possible applications for weather forecasting, in addition to tsunami warning (Kato et al. 2018).

In the near field too, innovative methods are being developed, such as those in Japan, where a very significant investment effort has encouraged the development of submarine cables composed of multi-technology sensors (Ohta 2012; Kawamoto et al. 2017; Inouye et al. 2019) in addition to GNSS buoys and conventional tide gauges. Similar experimental networks have also been deployed in the Pacific on the northwestern American coastline (e.g., the Neptune experiment, Thomson et al. 2011).

In conclusion, having GNSS buoys close to the coast would help to characterize the shoaling effect that is different depending on each specific bay or harbour. The parameters obtained from the analysis of continuous monitoring can then be put into operational numerical models relying on approximate amplification laws and providing forecasts in due time (Gailler et al. 2018).

6.8 The Promising Use of GNSS-TEC Data in Real Time

While GNSS data are practically already integrating early warning processes to retrieve the rupture pattern and the sea-level data (GNSS buoys), the TEC variations that are now often detected following large earthquakes and tsunamis are not yet operational. However, when detected through GNSS or altimetry data, they offer an interesting complementary constraint to characterize an ongoing tsunami, or even earlier, to estimate the possible efficiency of the tsunamigenic coupling. The number of events recorded through this technique is very tiny and the comprehensive analysis of the accuracy of the tsunami heights

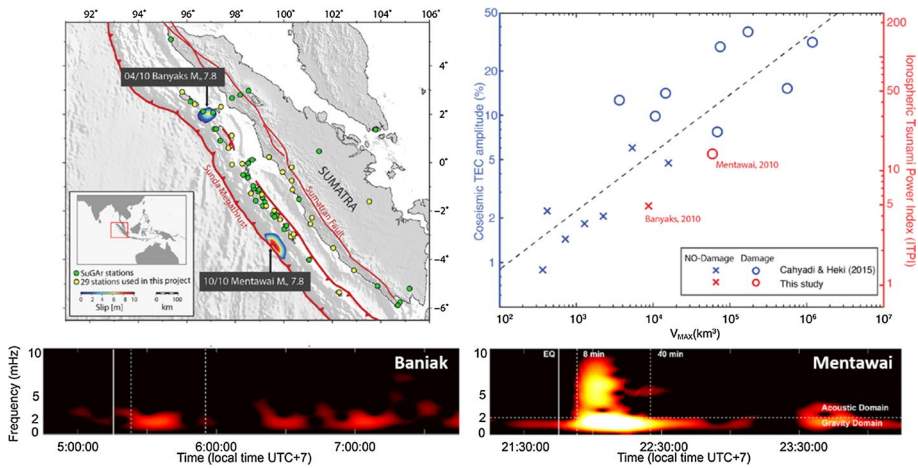


Fig. 18 Bottom: power density spectrum of the GNSS-TEC signals observed for Banyak (left) and Mentawai (right) events using the SuGAR (Sumatran GPS Array) network in Sumatra. The perturbations are 5% (left) and 15% (right) stronger than the mean background level. Top left: map showing epicentral areas of the April 2020 Mw 7.8 Banyak and October 2010 Mw 7.8 Mentawai earthquakes, and the 29 SuGAR stations used for the study (yellow dots). Top right: correlation V_{max} versus TEC amplitude/TECI. The V_{max} is obtained from the product of the maximum seafloor uplift and the rupture area (A), it corresponds to the maximum volume of displaced water. Figures adapted from Manta et al. (2020)

is not well established. To integrate early warning procedures, further check of all these aspects should be performed and guaranteed.

A recent study presented the case of the twin events of Banyak and Mentawai in Sumatra, in 2010 (Manta et al. 2020) (Fig. 18): both $M=7.8$ earthquakes were generated in the Sumatra mega thrust, and triggered a tsunami alert that was later cancelled. Unfortunately, the tsunami risk was underestimated in the case of the Mentawai event, and the resulting tsunami caused serious damage and more than 400 fatalities. The GNSS-TEC signature in the ionosphere of the AGW_{epi} highlights the important Mentawai uplift (causing the tsunami), compared to the Banyak event (Fig. 18 bottom).

A new TEC index (TECI) was introduced to estimate the energy transferred through the atmosphere (instead of the simple TEC amplitude used by previous authors) to better estimate the uplift and source extent (Fig. 18 top right). The link between the maximum volume of displaced water (V_{max}) and the TECI/Amplitude-TEC improves the reliability of ionospheric monitoring for tsunami risk estimation. Indeed, the TEC observations were previously only correlated with the magnitude of the event (Cahyadi and Heki 2015) or the coseismic uplift (Astafyeva et al. 2013), and not with the V_{max} directly related to the tsunami genesis. The fact that the Mentawai event was characterized as a slow earthquake amplifying the tsunami generation (a *tsunami earthquake*) (Newman et al. 2011) thus seems to be detectable through the TEC picture.

Other developments to rapidly locate the initial sea surface motion and estimate its amplitude accurately include TEC onset detection (Liu et al. 2010; Astafyeva et al. 2011) and rapid modelling of the near-field coseismic ionospheric pulse (Rolland et al. 2013; Mikesell et al. 2019).

Therefore, the double GNSS-derived observation of ground motion and TEC could be gradually included in future TWSs once the accuracy of the measurement is fully checked. The advantage of the double use of GNSS/TEC ionospheric monitoring during tsunami

genesis and ground motion is their synergy: the first is sensitive to the vertical sea floor displacement and the second to the slip at the source area.

6.9 Airglow

Ground-based airglow cameras also could help to monitor the arrival of tsunami waves, as soon as the wave characteristics of the detected signals can be fully determined in a few minutes. The successful observations of the IGW_{tsuna} by airglow cameras already mentioned open new technological perspectives in tsunami remote sensing by ground-based cameras and cameras on-board a satellite. Indeed, the CNES satellite project IONOGLOW is currently exploring the possibility of an airglow camera as a payload on a commercial GEO satellite to cover the entire Pacific Ocean and to complete the coverage of the airglow cameras on a global scale. This would overcome the limitation of the airglow cameras, which are currently restricted to localized, night-time measurements, but would require real-time processing to be useful during the warning process.

7 Conclusions and Perspectives

The striking development of satellite platforms since the middle of the 20th century has offered a revolutionary perspective on Earth imagery and global communications. The strong impulse given by the growing use of data acquired or transmitted by satellites has already produced key pictures and interpretations of physical processes at work on our planet, and also of the hazards it is exposed to. For tsunami hazards as well, they contribute to a better knowledge of the processes, to better preparedness, and they will undoubtedly become more and more incorporated in the monitoring and warning procedures of the future.

The 26 December 2004 Mw 9.1 Sumatra earthquake and resultant tsunami were devastating, claiming over 250,000 human lives in South and Southeast Asia. Following this disaster, the global awareness of tsunami exposure in these basins triggered the expansion of TWS for all regions (Bernard and Titov 2015). Meanwhile, since the 1990s, the use of massive electronic communication on a global scale has opened a new era to exchange data, warnings, procedures and scientific studies with large volumes of data involved. This was made possible through high-rate communications via the Internet, and using submarine cables and communication satellites, especially those in the Global Telecommunication System (GTS) from the World Meteorological Organization. Every single stage of a tsunami can thus now be monitored, thanks to data and communications taking advantage of satellites.

To summarize the various space data described in this paper, Table 1 presents their level of applicability regarding the different goals to be addressed. The fundamental role played by the satellite missions dedicated to transmission is underlined. Since the 1970s, satellites have been transmitting many types of geophysical and oceanographic data, in particular the sea-level data from Bottom Pressure Recorders (BPRs) (using Meteosat, Inmarsat, GTS, Iridium). Since the 1980s, high sampling rate seismic and geophysical data has been sent by Very Small Aperture Terminals (VSATs) from everywhere in the world. All these data are used either for source characterization and/or tsunami wave detection and measurement.

Table 1 Synthesis of the satellite missions described in this paper

Satellite mission	Source information	Early detection of tsunami	Sea-level measurement	Coastal impact	Prevention plan	Emergency management	Operational warning and forecast current/future
Altimetry	-	-	+	-	-	-	-/-
Optical imagery	++	-	-	+++	++	+	-/-
InSAR	+++	-	-	++	+	-	-/-
GNSS geodesy	++	-	-	++	++	++	+/++
GNSS buoy	-	+++	+++	-	-	+++	+/+++
GNSS-TEC	++	+	+	-	-	-	-/++
GRACE, GOCE	+	-	+	-	-	-	-/+
Airglow	++	+	+	-	-	-	-/+
Alert and data transmission	+++	+++	+++	-	-	+++	+++/>+++

The symbols reflect the efficiency for a given purpose, from low or non-applicable (-), to effective (+), very effective (++), and essential (+++)

For alert and warning communication, the downstream part of the warning system is currently using the Global Telecommunication system (GTS) implemented and managed by the World Meteorological Organization (WMO). For other applications, INMARSAT and Iridium are used, for example, by remote siren systems automatically triggered by satellite signals to reach remote communities and authorities who manage the information for alert and emergency management services. Cell broadcasts and alert systems to the population, such as developed in the federal emergency agency (FEMA) in the USA, are essentially relying on ground mobiles and antennas, but satellite operators participate in this emergency broadcasting as well.

Beyond this essential role of communication, satellites have played an increasing role in collecting the geophysical data. We have shown here that technologies for oceanography such as altimetry are not that efficient at monitoring tsunamis but, on the contrary, the most promising technique relies on ground-based receivers of GNSS signals. These offer an impressive capacity of detecting ground motions following an earthquake, which can be inverted in terms of source pattern, of monitoring sea-level variations when the receivers are installed on buoys, and finally of monitoring the upward ionospheric propagation of the tsunami signal through TEC signatures. Other applications such as GNSS-R remain to be confirmed with actual measures. The outstanding development of GNSS networks since the 1990s, with a growing number of real-time processing methods, offers a promising way of incorporating such data for operational purposes.

While many sensors dedicated to geophysical studies are developed within infrastructures or global networks to characterize and to warn, a growing number of less reliable sensors, but on very dense networks, can also bring an original complement to robust means. This is the case for the GNSS data acquired on ships and aircraft from commercial fleets that could also provide valuable, dense information across the oceans when a tsunami occurs (e.g., UNESCAP 2019). Although less secured and robust, they could increase the volume of data describing tsunami propagation, either of the direct waveform or its ionospheric signature.

As for the downstream component to populations and local authorities, satellite imagery helps for post-disaster surveys and for risk prevention plans. Though without direct physical relationship to global climate change, tsunamis are also more of a threat to shorelines where the mean sea level undergoes a gradual rise, exposing some areas with a low altitude above sea level to possible violent sea hazards. The continuous population density increase in coastal areas also contributes to the general increase of the tsunami risk in many places around the global ocean. Satellite data contributes to multi-hazard studies useful to mitigate tsunami impacts.

Finally, it is quite a paradox that the seafloor processes, such as those involving a rapid coseismic deformation, a landslide failure and a tsunami trigger, usually require expensive deployments in the sea (submarine cables, seafloor pressure gauges, ship cruises, etc.) not always available rapidly when a crisis occurs (e.g., monitoring seafloor ground deformation near Mayotte since 2018, e.g., Cesca et al. 2020). Although the satellite platforms contribute more and more to tsunami monitoring, the remote sensing within the oceanic layer remains an expensive challenge that should also be continuously supported for the sake of tsunami science and warnings.

Acknowledgements H. Hébert thanks the support given by the International Space Science Institute (Bern, Switzerland) to propose this review paper, which was originally presented in a solicited presentation at the multidisciplinary workshop held in April 2019 in Bern. Part of the work on the TEC data interpretation was supported by French ANR Cattell IONONAMI (Grant ANR-05-CATT-0004) project, and the TEC inversion and Pamatai airglow monitoring was developed within the NRL TWIST project. The altimetric swaths in

the Mediterranean were synthesized in the ANR RISKINAT MAREMOTI (Grant ANR-08-RISKINAT-05-01 project). The study on the design of a GNSS network in western Mediterranean areas has received funding from the EU FP7 project ASTARTE, Assessment, Strategy and Risk Reduction for Tsunamis in Europe grant No. 603839 (Project ASTARTE). The authors wish to thank two anonymous reviewers who helped to revise and improve the clarity of the paper, as well as the Guest Editor, Jérôme Benveniste, and the Editor in Chief, Michael Rycroft, for improving the English language.

References

- Abadie S, Harris JC, Grilli ST, Fabre R (2012) Numerical modelling of tsunami waves generated by the flankcollapse of the Cumbre Vieja Volcano (La Palma, Canary Islands): tsunami source and near field effects. *J Geophys Res Oceans* 117:C05030. <https://doi.org/10.1029/2011JC007646>
- Adriano B, Xia J, Baier G, Yokoya N, Koshimura S (2019) Multi-source data fusion based on ensemble learning for rapid building damage mapping during the 2018 Sulawesi Earthquake and Tsunami in Palu, Indonesia. *Remote Sens* 11:886. <https://doi.org/10.3390/rs11070886>
- Ajo-Franklin JB, Dou S, Lindsey NJ et al (2019) Distributed acoustic sensing using dark fiber for near-surface characterization and broadband seismic event detection. *Sci Rep* 9:1328. <https://doi.org/10.1038/s41598-018-36675-8>
- Ammon C, Kanamori H, Lay TA (2008) A great earthquake doublet and seismic stress transfer cycle in the central Kuril islands. *Nature* 451:561–565. <https://doi.org/10.1038/nature06521>
- Angove M, Arcas D, Bailey R, Carrasco P, Coetzee D, Fry B, Gledhill K, Harada S, von Hillebrandt-Andrade C, Kong L, McCreery C, McCurrach S-J, Miao Y, Sakya AE, Schindel F (2019) Ocean observations required to minimize uncertainty in global Tsunami forecasts, warnings, and emergency response. *Front Mar Sci* 6:350. <https://doi.org/10.3389/fmars.2019.00350>
- Artru J, Farges T, Lognonné P (2004) Acoustic waves generated from seismic surface waves: propagation properties determined from Doppler sounding observation and normal-mode modelling. *Geophys J Int* 158:1067–1077. <https://doi.org/10.1111/j.1365-246X.2004.02377.x>
- Artru J, Ducic V, Kanamori H, Lognonné P, Murakami M (2005) Ionospheric detection of gravity waves induced by tsunamis. *Geophys J Int* 160(3):840–848. <https://doi.org/10.1111/j.1365-246X.2005.02552.x>
- Assier-Rzadkiewicz S, Mariotti C, Heinrich P (1997) Numerical simulation of submarine landslides and their hydraulic effects. *J Waterway Port Coast Ocean Eng* 123(4):149–157. [https://doi.org/10.1061/\(ASCE\)0733-950X\(1997\)123:4\(149\)](https://doi.org/10.1061/(ASCE)0733-950X(1997)123:4(149))
- Astafyeva E (2019) Ionospheric detection of natural hazards. *Rev Geophys*. <https://doi.org/10.1029/2019RG000668>
- Astafyeva E, Lognonné P, Rolland L (2011) First ionosphere images for the seismic slip of the Tohoku-oki earthquake. *Geophys Res Lett* 38:L22104. <https://doi.org/10.1029/2011GL049623>
- Astafyeva E, Shalimov S, Olshanskaya E, Lognonné P (2013) Ionospheric response to earthquakes of different magnitudes: larger quakes perturb the ionosphere stronger and longer. *Geophys Res Lett* 40(9):1675–1681. <https://doi.org/10.1002/grl.50398>
- Bai Y, Gao C, Singh S, Koch M, Adriano B, Mas E, Koshimura S (2018) A framework of rapid regional tsunami damage recognition from post-event TerraSAR-X imagery using deep neural networks. *IEEE Geosci Remote S* 15(1):43–47. <https://doi.org/10.1109/lgrs.2017.2772349>
- Barrientos S, National Seismological Center (CSN) team (2018) The seismic network of Chile. *Seismological Res Lett* 89(2A):467–474. <https://doi.org/10.1785/0220160195>
- Bernard E (2001) Tsunami: reduction of impacts through three key actions (TROIKA). In: Proceedings of the international tsunami symposium 2001 (ITS 2001), Session 1-1, Seattle, WA, 7–10 August 2001, pp 247–262. https://www.pmel.noaa.gov/pubs/docs/ITS2001/1-01_Bernard.pdf. Accessed Aug 2020
- Bernard E, Titov V (2015) Evolution of tsunami warning systems and products. *Philos Trans R Soc A* 373:20140371. <https://doi.org/10.1098/rsta.2014.0371>
- Bessette-Kirton E, Allstadt K, Godt J, Pursley J (2017) Preliminary analysis of satellite imagery and seismic observations of the Nuugaatsiaq Landslide and Tsunami, Greenland, U.S. Geological Survey—Landslide Hazards Program. <https://www.usgs.gov/natural-hazards/landslide-hazards/science/preliminary-analysis-satellite-imagery-and-seismic>. Last accessed Aug 2020
- Bessis J-L, Béguignon J, Mahmood A (2004) The international charter “space and major disasters” initiative. *Acta Astronaut* 54(3):183–190. [https://doi.org/10.1016/S0094-5765\(02\)00297-7](https://doi.org/10.1016/S0094-5765(02)00297-7)
- Bilitza D, Rawer K (1996) International reference ionosphere. In: Dieminger W, Hartmann G, Leitinger R (eds) *The upper atmosphere—data analysis and interpretation*. Springer, Berlin, pp 735–772

- Blanc E, Ceranna L, Hauchecorne A et al (2018) Toward an improved representation of middle atmospheric dynamics thanks to the ARISE Project. *Surv Geophys* 39:171–225. <https://doi.org/10.1007/s10712-017-9444-0>
- Bonaccorso A, Gambino S, Mattia M, Guglielmino F, Puglisi G, Boschi E (2009) Insight on recent Stromboli eruption inferred from terrestrial and satellite ground deformation measurements. *J Volcanol Geoth Res* 18:172–181. <https://doi.org/10.1016/j.jvolgeores.2009.01.007>
- Borrero JC, Synolakis CE, Fritz HM (2006) Northern Sumatra field surveys after the December 2004 great Sumatra earthquake and Indian Ocean tsunami. *Earthq Spectra* 22(S3):S93–S104. <https://doi.org/10.1193/1.2206793>
- Broutman D, Eckermann SD, Drob DP (2014) The partial reflection of tsunami-generated gravity waves. *J Atmos Sci* 71:3416–3426. <https://doi.org/10.1175/JAS-D-13-0309.1>
- Bürgmann R, Chadwell D (2014) Seafloor geodesy. *Annu Rev Earth Planet Sci* 42:509–534. <https://doi.org/10.1146/annurev-earth-060313-054953>
- Cahyadi MN, Heki K (2015) Coseismic ionospheric disturbance of the large strike-slip earthquakes in North Sumatra in 2012: Mw dependence of the disturbance amplitudes. *Geophys J Int* 200:116–129. <https://doi.org/10.1093/gji/ggu343>
- Caplan-Auerbach J, Fox CG, Duennebiele FK (2001) Hydroacoustic detection of submarine landslides on Kilauea Volcano. *Geophys Res Lett* 28:1811–1813. <https://doi.org/10.1029/2000GL012545>
- Carlà T, Intrieri E, Di Traglia F, Casagli N (2016) A statistical-based approach for determining the intensity of unrest phases at Stromboli volcano (Southern Italy) using one-step-ahead forecasts of displacement time series. *Nat Hazard* 84:669–683. <https://doi.org/10.1007/s11069-016-2451-5>
- Carlà T, Intrieri E, Raspini F, Bardi F, Farina P, Ferretti A, Colombo D, Novali F, Casagli N (2019a) Perspectives on the prediction of catastrophic slope failures from satellite InSAR. *Sci Rep* 9:14137. <https://doi.org/10.1038/s41598-019-50792-y>
- Carlà T, Tofani V, Lombardi L, Raspini F, Bianchini S, Bertolo D, Thuegatz P, Casagli N (2019b) Combination of GNSS, satellite InSAR, and GBInSAR remote sensing monitoring to improve the understanding of a large landslide in high alpine environment. *Geomorphology* 335:62–75. <https://doi.org/10.1016/j.geomorph.2019.03.014>
- Cesca S, Letort J, Razafindrakoto HNT et al (2020) Drainage of a deep magma reservoir near Mayotte inferred from seismicity and deformation. *Nat Geosci* 13:87–93. <https://doi.org/10.1038/s41561-019-0505-5>
- Chao WA, Wu TR, Ma KF, Kuo YT, Wu YM, Zhao L, Chung MJ, Wu H, Tsai YL (2018) The large Greenland landslide of 2017: Was a tsunami warning possible? *Seismol Res Lett* 89:1335–1344. <https://doi.org/10.1785/0220170160>
- Chen P, Liew SC, Kwok LK (2006) Tsunami damage mapping and assessment in Sumatra using remote sensing and GIS techniques. In: *Proceedings of IEEE international conference on geoscience and remote sensing symposium, 2006 July 31–August 4, Denver, CO*, pp 297–300. <https://doi.org/10.1109/IGARSS.2006.81>
- Clément J, Raymond D (2015) New tsunami forecast tools for the French Polynesia Tsunami warning system. *Pure appl Geophys* 172:791–804. <https://doi.org/10.1007/s00024-014-0888-6>
- Coisson P, Occhipinti G, Lognonné P, Rolland LM (2011) Tsunami signature in the ionosphere: the innovative role of OTH radar. *Radio Sci*. <https://doi.org/10.1029/2010RS004603>
- Coisson P, Lognonné P, Walwer D, Rolland LM (2015) First tsunami gravity wave detection in ionospheric radio occultation data. *Earth Space Sci* 2:125–133. <https://doi.org/10.1002/2014EA000054>
- Duputel Z, Rivera L, Kanamori H, Hayes GP, Hirsorn B, Weinstein S (2011) Real-time W phase inversions during the 2011 Tohoku-oki earthquake. *Earth Planets Space* 63:535–539. <https://doi.org/10.5047/eps.2011.05.032>
- Elliott JR, Walters RJ, Wright TJ (2016) The role of space-based observation in understanding and responding to active tectonics and earthquakes. *Nat Commun* 7:13844. <https://doi.org/10.1038/ncomms13844>
- Endo Y, Adriano B, Ma Koshimura S (2018) New insights into multiclass damage classification of tsunami-induced building damage from SAR images. *Remote Sens* 10:2059. <https://doi.org/10.3390/rs10122059>
- Fritz HM, Hager WH, Minor H-E (2004) Near field characteristic of landslide generated impulse waves. *J Waterway Port C Div* 130:287–302. [https://doi.org/10.1061/\(ASCE\)0733-950X\(2004\)130:6\(287\)](https://doi.org/10.1061/(ASCE)0733-950X(2004)130:6(287))
- Gaffet S, Guglielmi Y, Cappa F, Pambrun C, Monfret T, Amiran D (2010) Use of the simultaneous seismic, GPS and meteorological monitoring for the characterization of a large unstable mountain slope in the southern French Alps. *Geophys J Int* 182(3):1395–1410. <https://doi.org/10.1111/j.1365-246X.2010.04683.x>

- Gailler A, Hébert H, Loevenbruck A, Hernandez B (2013) Simulation systems for tsunami wave propagation forecasting within the French tsunami warning center. *Nat Hazard Earth Sys* 13:2465–2482. <https://doi.org/10.5194/nhess-13-2465-2013>
- Gailler A, Hébert H, Schindelé F, Reymond D (2018) Coastal amplification laws for the french tsunami warning center: numerical modeling and fast estimate of tsunami wave heights along the French Riviera. *Pure appl Geophys* 175:1429. <https://doi.org/10.1007/s00024-017-1713-9>
- Galvan D, Komjathy A, Hickey MP, Mannucci AJ (2011) The 2009 Samoa and 2010 tsunamis as observed in the ionosphere using GPS total electron content. *J Geophys Res-Space* 116(6):A06318. <https://doi.org/10.1029/2010JA016204>
- Garcia RF, Doornbos E, Bruinsma S, Hébert H (2014) Atmospheric gravity waves due to the Tohoku-Oki tsunami observed in the thermosphere by GOCE. *J Geophys Res Atmos* 119:4498–4506. <https://doi.org/10.1002/2013JD021120>
- Glimsdal S, Pedersen GK, Harbitz CB, Løvholt F (2013) Dispersion of tsunamis: Does it really matter? *Nat Hazards Earth Syst Sci* 13:1507–1526. <https://doi.org/10.5194/nhess-13-1507-2013>
- González FI, Bernard EN, Meinig C, Eble MC, Mojfeld HO, Stalin S (2005) The NTHMP tsunami network. *Nat Hazards* 35:25. <https://doi.org/10.1007/s11069-004-2402-4>
- Grandin R, Klein E, Métois M, Vigny C (2016) Three-dimensional displacement field of the 2015 Mw 8.3 Illapel earthquake (Chile) from across- and along-track Sentinel-1 TOPS interferometry. *Geophys Res Lett* 43:2552–2561. <https://doi.org/10.1002/2016GL067954>
- Grawe MA, Makela JJ (2015) The ionospheric responses to the 2011 Tohoku, 2012 Haida Gwaii, and 2010 Chile tsunamis: effects of tsunami orientation and observation geometry. *Earth Space Sci* 2:472–483. <https://doi.org/10.1002/2015EA000132>
- Grawe MA, Makela JJ (2017) Observation of tsunami-generated ionospheric signatures over Hawaii caused by the 16 September 2015 Illapel earthquake. *J Geophys Res Space Phys* 122:1128–1136. <https://doi.org/10.1002/2016JA023228>
- Guérin C, Binet R, Pierrot-Deseilligny M (2014) Automatic detection of elevation changes by differential DSM analysis: application to urban areas. *IEEE J Sel Top Appl* 7(10):4020–4037. <https://doi.org/10.1109/JSTARS.2014.2300509>
- Gupta HK (2005) Mega-tsunami of 26th December, 2004: Indian initiative for early warning system and mitigation of oceanogenic hazards. *Episodes* 28(1):2–5
- Gupta HK (2008) India's initiative in mitigating tsunami and storm surge hazard. *J Earthq Tsunami* 2(4):287–295
- Gupta HK, Gahalaut VK (2015) Seismotectonics and large earthquake generation in the Himalayan region. *Gondwana Res* 25(1):204–213. <https://doi.org/10.1016/j.gr.2012.11.006>
- Hébert H, Heinrich P, Schindelé F, Piatanesi A (2001) Far-field simulation of tsunami propagation in the Pacific Ocean: impact on the Marquesas Islands (French Polynesia). *J Geophys Res* 106(C5):9161–9177. <https://doi.org/10.1029/2000JC000552>
- Hébert H, Sladen A, Schindelé F (2007) Numerical modeling of the Great 2004 Indian Ocean Tsunami: focus on the Mascarene Islands. *Bull Seismol Soc Am* 97(1A):S208–S222. <https://doi.org/10.1785/0120050611>
- Hébert H, Burg P-E, Binet R, Lavigne F, Allgeyer S, Schindelé F (2012) The 2006 July 17 Java (Indonesia) tsunami from satellite imagery and numerical modelling: a single or complex source? *Geophys J Int* 191(3):1255–1271. <https://doi.org/10.1111/j.1365-246X.2012.05666.x>
- Heinrich P, Piatanesi A, Hébert H (2001) Numerical modelling of tsunami generation and propagation from submarine slumps: the 1998 Papua New Guinea event. *Geophys J Int* 145(1):97–111. <https://doi.org/10.1111/j.1365-246X.2001.00336.x>
- Hickey MP, Schubert G, Walterscheid RL (2009) Propagation of tsunami-driven gravity waves into the thermosphere and ionosphere. *J Geophys Res* 114:A08304. <https://doi.org/10.1029/2009JA014105>
- Hickey MP, Walterscheid RL, Schubert G (2010a) Wave mean flow interactions in the thermosphere induced by a major tsunami. *J Geophys Res* 115:A09309. <https://doi.org/10.1029/2009JA014927>
- Hickey MP, Schubert G, Walterscheid RL (2010b) Atmospheric airglow fluctuations due to a tsunami driven gravity wave disturbance. *J Geophys Res* 115:A06308. <https://doi.org/10.1029/2009JA014977>
- Howe BM et al (2019) SMART cables for observing the global ocean: science and implementation. *Front Mar Sci* 6:24. <https://doi.org/10.3389/fmars.2019.00424>
- Huba JD, Drob DP, Wu T-W, Makela JJ (2015) Modeling the ionospheric impact of tsunami-driven gravity waves with SAMI3: conjugate effects. *Geophys Res Lett* 42:5719–5726. <https://doi.org/10.1002/2015GL064871>
- Hupe P, Ceranna L, Le Pichon A (2019) How can the international monitoring system infrasound network contribute to gravity wave measurements? *Atmosphere* 10(7):399. <https://doi.org/10.3390/atmos10070399>

- Inouye M, Tanioka Y, Yamanaka Y (2019) Method for near-real time estimation of tsunami sources using ocean bottom pressure sensor network (S-Net). *Geosciences* 9:310. <https://doi.org/10.3390/geosciences9070310>
- IOC (Intergovernmental Oceanographic Commission) (1965) International coordination group for the tsunami warning system in the Pacific (ICG/ITSU), IOC 4th Session, Resolution IV-6
- IOC (Intergovernmental Oceanographic Commission) (2005a) Intergovernmental coordination group for the Indian Ocean Tsunami warning and mitigation system, IOC 23rd Session, Resolution XXIII-12
- IOC (Intergovernmental Oceanographic Commission) (2005b) Establishment of an intergovernmental coordination group for tsunami and other coastal hazards warning system for the Caribbean and adjacent regions, IOC 23rd Session, Resolution XXIII-13
- IOC (Intergovernmental Oceanographic Commission) (2005c) Intergovernmental coordination group for a tsunami early warning system in the North-eastern Atlantic and the mediterranean and connected seas (ICG/NEAMTWS), IOC 23rd Session, Resolution XXIII-14
- Iyyappan M, Usha T, Ramakrishnan SS et al (2018) Evaluation of tsunami inundation using synthetic aperture radar (SAR) data and numerical modeling. *Nat Hazards* 92:1419. <https://doi.org/10.1007/s11069-018-3257-4>
- Jamelot A, Reymond D (2015) New Tsunami forecast tools for the French Polynesia tsunami warning system part II: numerical modelling and tsunami height estimation. *Pure appl Geophys* 172:805. <https://doi.org/10.1007/s00024-014-0997-2>
- Jamelot A, Gailler A, Heinrich P, Vallage A, Champenois J (2019) Tsunami Simulations of the Sulawesi Mw 7.5 event: comparison of seismic sources issued from a Tsunami warning context versus post-event finite source. *Pure appl Geophys* 176:3351–3376. <https://doi.org/10.1007/s00024-019-02274-5>
- Ji Y, Sri Sumantyo JT, Chua MY, Waqar MM (2018) Earthquake/Tsunami damage assessment for urban areas using post-event PolSAR data. *Remote Sens* 10:1088. <https://doi.org/10.3390/rs10071088>
- Jin S (2019) GNSS atmospheric seismology: theory, observations and modelling. Springer, Singapore. <https://doi.org/10.1007/978-981-10-3178-6>
- Jin S, Occhipinti G, Jin R (2015) GNSS ionospheric seismology: recent observation evidences and characteristics. *Earth Sci Rev* 147:54–64. <https://doi.org/10.1016/j.earscirev.2015.05.003>
- JMA, Japanese Meteorological Agency (2013) Lessons learned from the tsunami disaster caused by the 2011 Great East Japan Earthquake and improvements in JMA's tsunami warning system. http://www.data.jma.go.jp/svd/eqev/data/en/tsunami/LessonsLearned_Improvements_brochure.pdf. Last accessed August 2020
- Kanamori H (1972) Mechanism of tsunami earthquakes. *Phys Earth Planet Int* 6(5):346–359. [https://doi.org/10.1016/0031-9201\(72\)90058-1](https://doi.org/10.1016/0031-9201(72)90058-1)
- Kanamori H, Rivera L (2008) Source inversion of W phase: speeding up seismic tsunami warning. *Geophys J Int* 175(1):222–238. <https://doi.org/10.1111/j.1365-246X.2008.03887.x>
- Kato T, Terada Y, Nagai T, Koshimura S (2010) Tsunami monitoring system using GPS buoy: present status and outlook. *IEEE Int Geosci Remote Se.* <https://doi.org/10.1109/IGARSS.2010.5654449>
- Kato T, Terada Y, Tadokoro K, Kinugasa N, Futamura A, Toyoshima M, Yamamoto S, Ishii M, Tsugawa T, Nishioka M, Takizaka K, Shoji Y, Seka H (2018) Development of GNSS buoy for a synthetic geohazard monitoring system. *J Disaster Res* 13(3):460–471. <https://doi.org/10.20965/jdr.2018.p0460>
- Kawai H, Satoh M, Miyata M, Kobayashi T (2012) 2010 Chilean Tsunami observed by NOWPHAS GPS buoys, seabed wave gauges and coastal tide gauges. *Int J Offshore Polar Eng* 22(3):177–185
- Kawamoto S, Ohta Y, Hiyama Y, Todoriki M, Nishimura T, Furuya T, Sato Y, Yahagi T, Miyagawa K (2017) REGARD: a new GNSS-based real-time finite fault modeling system for GEONET. *J Geophys Res* 122:1324–1349. <https://doi.org/10.1002/2016JB013485>
- Kerr RA (2005) Model shows islands muted tsunami after latest Indonesian Quake. *Science* 308(5720):341. <https://doi.org/10.1126/science.308.5720.341a>
- Kherani EA, Lognonné P, Hébert H, Rolland L, Astafyeva E, Occhipinti G, Coisson P, Walwer D, de Paula ER (2012) Modelling of the total electronic content and magnetic field anomalies generated by the 2011 Tohoku-Oki tsunami and associated acoustic-gravity waves. *Geophys J Int* 191:1049–1066. <https://doi.org/10.1111/j.1365-246X.2012.05617.x>
- Kherroubi A, Déverchère J, Yelles A, Mercier de Lépinay B, Domzig A, Cattaneo A, Bracène R, Gaullier V, Graindorge D (2009) Recent and active deformation pattern off the easternmost Algerian margin, Western Mediterranean Sea: new evidence for contractional tectonic reactivation. *Mar Geol* 261(1–4):17–32. <https://doi.org/10.1016/j.margeo.2008.05.016>
- Kong LSL, Dunbar PK, Arcos N (eds) (2015) Pacific Tsunami warning system: a half century of protecting the Pacific (1965–2015). International Tsunami Information Center, Government Printing Office, 188 pp

- Labbé M, Donnadiou C, Daubord C, Hébert H (2012) Refined numerical modeling of the 1979 tsunami in Nice (French Riviera): comparison with coastal data. *J Geophys Res-Earth* 117:F01008. <https://doi.org/10.1029/2011JF001964>
- Lavigne F, Paris R, Grancher D, Wassmer P, Brunstein D, Vautier F, Leone F, Flohic F, De Coster B, Gunawan T, Gomez C, Setiawan A, Cahyadi R, Fachrizal A (2009) Reconstruction of tsunami inland propagation on December 26, 2004 in Banda Aceh, Indonesia, through field investigations. *Pure appl Geophys* 13(166):259–281. <https://doi.org/10.1007/s00024-008-0431-8>
- Lay T, Kanamori H, Ammon CJ, Nettles M, Ward SN, Aster RC, Beck SL, Bilek SL, Brudzinski MR, Butler R, DeShon HR, Ekström G, Satake K, Sipkin S (2005) The Great Sumatra-Andaman Earthquake of 26 December 2004. *Science* 308:1127–1133. <https://doi.org/10.1126/science.1112250>
- Lay T, Ammon C, Kanamori H, Rivera L, Koper KD, Hutko AR (2010) The 2009 Samoa-Tonga great earthquake triggered doublet. *Nature* 466:964–968. <https://doi.org/10.1038/nature09214>
- Le Pichon A, Herry P, Mialle P, Vergoz J, Brachet N, Garcés M, Drob D, Ceranna L (2005) Infrasound associated with 2004–2005 large Sumatra earthquakes and tsunami. *Geophys Res Lett* 32:L19802. <https://doi.org/10.1029/2005GL023893>
- Leone F, Lavigne F, Paris R, Denain J-C, Vinet F (2010) A spatial analysis of the December 26th, 2004 tsunami-induced damages: lessons learned for a better risk assessment integrating buildings vulnerability. *Appl Geogr* 31(1):363–375. <https://doi.org/10.1016/j.apgeog.2010.07.009>
- Li J, Zhang H, Hou P, Fu B, Zheng G (2016) Mapping the bathymetry of shallow coastal water using single-frame fine-resolution optical remote sensing imagery. *Acta Oceanol Sin* 35(1):60–66. <https://doi.org/10.1007/s13131-016-0797-x>
- Liu JY, Tsai HF, Lin CH, Kamogawa M, Chen YI, Lin CH et al (2010) Coseismic ionospheric disturbances triggered by the Chi-Chi earthquake. *J Geophys Res Space Phys* 115(A8):A08303. <https://doi.org/10.1029/2009JA014943>
- Lognonné P (2009) Seismic waves from atmospheric sources and atmospheric/ionospheric signatures of seismic waves, Chapter 10. In: Le Pichon A (ed) *Infrasound monitoring for atmospheric studies*, Springer, New-York. https://doi.org/10.1007/978-1-4020-9508-5_10
- Lognonné P, Clévéde E, Kanamori H (1998) Normal mode summation of seismograms and barograms in an spherical Earth with realistic atmosphere. *Geophys J Int* 135:388–406. <https://doi.org/10.1046/j.1365-246X.1998.00665.x>
- Lognonné P, Artru J, Garcia R, Crespon F, Ducic V, Jeansou E, Occhipinti G, Helbert J, Moreaux G, Godet P-E (2006) Ground based GPS tomography of ionospheric post-seismic signal. *Planet Space Sci* 54:528–540. <https://doi.org/10.1016/j.pss.2005.10.021>
- Løvholt F, Pedersen G, Harbitz CB, Glimsdal S, Kim J (2015) On the characteristics of landslide tsunamis. *Philos Trans R Soc A* 373:20140376. <https://doi.org/10.1098/rsta.2014.0376>
- Lynett PJ et al (2017) Inter-model analysis of tsunami-induced coastal currents. *Ocean Model* 114:14–32. <https://doi.org/10.1016/j.ocemod.2017.04.003>
- Ma S, Tao Z, Yang X, Yu Y, Zhou X, Li Z (2014) Bathymetry retrieval from hyperspectral remote sensing data in optical-shallow water. *IEEE T Geosci Remote* 52(2):1205–1212. <https://doi.org/10.1109/TGRS.2013.2248372>
- Mader CL, Curtis G (1991) Modeling Hilo, Hawaii tsunami inundation. *Sci Tsunami Hazard* 9:85–94
- Mai C-L, Kiang J-F (2009) Modeling of ionospheric perturbation by 2004 Sumatra tsunami. *Radio Sci*. <https://doi.org/10.1029/2008RS004060>
- Makela JJ, Lognonné P, Hébert H, Gehrels T, Rolland L, Allgeyer S, Kherani A, Occhipinti G, Astafyeva E, Coisson P, Loevenbruck A, Clévéde E, Kelley MC, Lamouroux J (2011) Imaging and modeling the ionospheric airglow response over Hawaii to the tsunami generated by the Tohoku earthquake of 11 March 2011. *Geophys Res Lett*. <https://doi.org/10.1029/2011GL047860>
- Mangeney A, Heinrich P, Roche R, Boudon G, Cheminée J (2000) Modeling of debris avalanche and generated water waves: application to real and potential events in Montserrat. *Phys Chem Earth Pt A* 25(9–11):741–745. [https://doi.org/10.1016/S1464-1895\(00\)00115-0](https://doi.org/10.1016/S1464-1895(00)00115-0)
- Mannucci AJ, Wilson BD, Yuan DN, Ho CH, Lindqwister UJ, Runge TF (1998) A global mapping technique for GPS-derived ionospheric total electron content measurements. *Radio Sci* 33:565–582. <https://doi.org/10.1029/97RS020707>
- Manta F, Occhipinti G, Feng L, Hill EM (2020) Rapid identification of tsunami earthquakes using GPS ionospheric sounding. *Sci Rep* 10:11054. <https://doi.org/10.1038/s41598-020-68097-w>
- Martin-Neira M (1993) A passive reflectometry and interferometry system (PARIS): application to ocean altimetry. *ESA J* 17:331–355. <https://doi.org/10.1109/36.898676>
- Martin-Neira M, Colmenarejo P, Ruffini G, Serra C (2002) Altimetry precision of 1 cm over a pond using the wide-lane carrier phase of GPS reflected signals. *Can J Remote Sens* 28:394–403. <https://doi.org/10.5589/m02-039>

- Marty J (2019) The IMS infrasound network: current status and technological developments. In: Le Pichon A, Blanc E, Hauchecorne A (eds) *Infrasound monitoring for atmospheric studies*. Springer, Cham. https://doi.org/10.1007/978-3-319-75140-5_1
- Meilianda E, Pradhan B, Syamsidik S, Comfort L, Alfian D, Juanda R, Syahreza S, Munadi K (2019) Assessment of post-tsunami disaster land use/land cover change and potential impact of future sea-level rise to low-lying coastal areas: a case study of Banda Aceh coast of Indonesia. *Int J Disaster Risk Reduct* 41:101292. <https://doi.org/10.1016/j.ijdr.2019.101292>
- Melgar D, Hayes GP (2019) Characterizing large earthquakes before rupture is complete. *Sci Adv*. <https://doi.org/10.1126/sciadv.aav2032>
- Meng X, Komjathy A, Verkhoglyadova OP, Yang Y-M, Deng Y, Mannucci AJ (2015) A new physics-based modeling approach for tsunami-ionosphere coupling. *Geophys Res Lett* 42:4736–4744. <https://doi.org/10.1002/2015GL064610>
- Meng X, Verkhoglyadova OP, Komjathy A, Savastano G, Mannucci AJ (2018) Physics-based modeling of earthquake-induced ionospheric disturbances. *J Geophys Res Space Phys* 123:8021–8038. <https://doi.org/10.1029/2018JA025253>
- Mikesell T, Rolland L, Lee R, Zedek F, Coisson P, Dessa J-X (2019) IonoSeis: a package to model coseismic ionospheric disturbances. *Atmosphere* 10(8):443. <https://doi.org/10.3390/atmos10080443>
- Milburn HB, Nakamura AI, González FI (1996) Real-time tsunami reporting from the deep ocean. In: *Proceedings of the oceans 96 MTS/IEEE conference*, 23–26 September 1996, Fort Lauderdale, FL, pp 390–394. <https://doi.org/10.1109/oceans.1996.572778>
- Mohammed F, Fritz HM (2012) Physical modeling of tsunamis generated by three-dimensional deformable granular landslides. *J Geophys Res* 117:C11015. <https://doi.org/10.1029/2011JC007850>
- Moreno M, Rosenau M, Oncken O (2010) 2010 Maule earthquake slip correlates with pre-seismic locking of Andean subduction zone. *Nature* 467:198–202. <https://doi.org/10.1038/nature09349>
- Nayak S, Srinivas Kumar T (2008a) Indian Tsunami warning system. In: *The international archives of the photogrammetry. Remote sensing and spatial information sciences XXXVII, Part B4*, Beijing, pp 1501–1506
- Nayak S, Srinivasa Kumar T (2008b) The first tsunami warning centre in the Indian ocean. In: *Risk wise*, Tudor Rose Publishers, UK, pp 175–177
- NCEI (National Centers for Environmental Informations) (2017) Tsunami sources 1610 B.C. to A.D. 2017 from earthquakes, volcanic eruptions, landslides, and other causes, International Tsunami Information Center. http://itc.ioc-unesco.org/images/stories/awareness_and_education/map_posters/2017_tsu_poster_20180313_a2_low_res.pdf
- Newman AV, Hayes G, Wei Y, Convers J (2011) The 25 October 2010 Mentawai tsunami earthquake, from real-time discriminants, finite-fault rupture, and tsunami excitation. *Geophys Res Lett* 38:L05302. <https://doi.org/10.1029/2010GL046498>
- NOWPHAS, Nationwide Ocean Wave information network for Ports and HarbourS. <https://nowphas.mlit.go.jp/>. Last accessed Aug 2020
- Occhipinti G (2015) The seismology of the planet mongo. In: Morra G, Yuen DA, King D, Lee S, Stein S (eds) *Subduction dynamics*. <https://doi.org/10.1002/9781118888865.ch9>
- Occhipinti G, Lognonné P, Kherani EA, Hébert H (2006) Three-dimensional waveform modeling of ionospheric signature induced by the 2004 Sumatra tsunami. *Geophys Res Lett*. <https://doi.org/10.1029/2006GL026865>
- Occhipinti G, Kherani EA, Lognonné P (2008) Geomagnetic dependence of ionospheric disturbances induced by tsunamigenic internal gravity waves. *Geophys J Int* 173(3):753–765. <https://doi.org/10.1111/j.1365-246X.2008.03760.x>
- Occhipinti G, Dorey P, Farges T, Lognonné P (2010) Nostradamus: the radar that wanted to be a seismometer. *Geophys Res Lett* 37:L18104. <https://doi.org/10.1029/2010GL044009>
- Occhipinti G, Coisson P, Makela JJ, Allgeyer S, Kherani A, Hébert H, Lognonné P (2011) Three-dimensional numerical modeling of tsunami-related internal gravity waves in the Hawaiian atmosphere. *Earth Planets Space* 63(7):847–851. <https://doi.org/10.5047/eps.2011.06.051>
- Occhipinti G, Rolland L, Lognonné P, Watada S (2013) From Sumatra 2004 to Tohoku-Oki 2011: the systematic GPS detection of the ionospheric signature induced by tsunamigenic earthquakes. *J Geophys Res Space* 118:3626–3636. <https://doi.org/10.1002/jgra.50322>
- Occhipinti G, Aden-Antoniow F, Bablet A et al (2018) Surface waves magnitude estimation from ionospheric signature of Rayleigh waves measured by Doppler sounder and OTH radar. *Sci Rep* 8:1555. <https://doi.org/10.1038/s41598-018-19305-1>
- Ohta Y (2012) Quasi real-time fault model estimation for near-field tsunami forecasting based on RTK-GPS analysis: application to the 2011 Tohoku-Oki earthquake (Mw9.0). *J Geophys Res*. <https://doi.org/10.1029/2011JB008750>




- Ohta Y, Inoue T, Koshimura S, Kawamoto S, Hino R (2018) Role of real-time GNSS in near-field tsunami forecasting. *J Disaster Res* 13:453–459. <https://doi.org/10.20965/jdr.2018.p0453>
- Okada Y (1985) Surface deformation due to shear and tensile faults in a half-space. *B Seismol Soc Am* 75(4):1135–1154
- Okal EA, Piatanesi A, Heinrich P (1999) Tsunami detection by satellite altimetry. *J Geophys Res* 104:599–615. <https://doi.org/10.1029/1998JB000018>
- Ozaki T (2012) JMA's Tsunami warning for the 2011 Great Tohoku earthquake and Tsunami improvement plan. *J Disaster Res* 7:439–445. <https://doi.org/10.20965/jdr.2012.p0439>
- Ozawa S, Nishimura T, Suito H, Kobayashi T, Tobita M, Imakiire T (2011) Coseismic and postseismic slip of the 2011 magnitude-9 Tohoku-Oki earthquake. *Nature* 475:373–376. <https://doi.org/10.1038/nature10227>
- Paris A, Okal EA, Guérin C, Heinrich P, Schindelé F, Hébert H (2019) Numerical modeling of the June 17, 2017 landslide and Tsunami events in Karrat Fjord, West Greenland. *Pure appl Geophys* 176(7):3035–3057. <https://doi.org/10.1007/s00024-019-02123-5>
- Paris A, Heinrich P, Paris R, Abadie S (2020) The December 22, 2018 Anak Krakatau, Indonesia, landslide and tsunami: preliminary modeling results. *The December 22, 2018 Anak Krakatau, Indonesia, landslide and tsunami: preliminary modeling results. Pure appl Geophys* 177:571–590. <https://doi.org/10.1007/s00024-019-02394-y>
- Percival DB, Denbo DW, Gica E, Huang PY, Mofield HO, Spillane MC, Titov VV (2018) Evaluating the effectiveness of DART® Buoy networks based on forecast accuracy. *Pure appl Geophys* 175:1445. <https://doi.org/10.1007/s00024-018-1824-y>
- Polcari M, Albano M, Montuori A, Bignami C, Tolomei C, Pezzo G, Falcone S, La Piana C, Doumaz F, Salvi S, Stramondo S (2018) InSAR monitoring of Italian coastline revealing natural and anthropogenic ground deformation phenomena and future perspectives. *Sustainability* 10(9):3152. <https://doi.org/10.3390/su10093152>
- Poupardin A, de Michele M, Raucoles D, Idier D (2014) Water depth inversion from satellite dataset. *IEEE Geosci Remote Sens Symp* 54(4):2329–2342. <https://doi.org/10.1109/IGARSS.2014.6946924>
- Poupardin A, Heinrich P, Frère A, Imbert D, Hébert H, Flouzat M (2017) The 1979 submarine landslide-generated tsunami in Mururoa, French Polynesia. *Pure Appl Geoph* 174(8):3293–3311. <https://doi.org/10.1007/s00024-016-1464-z>
- Puglisi G, Bonaccorso A, Mattia M, Aloisi M, Bonforte A, Campisi O, Cantarero M, Falzone G, Puglisi B, Rossi M (2005) New integrated geodetic monitoring system at Stromboli volcano (Italy). *Eng Geol* 79(1–2):13–31. <https://doi.org/10.1016/j.enggeo.2004.10.013>
- Raharja R, Gunawan E, Meilano I et al (2016) Long aseismic slip duration of the 2006 Java tsunami earthquake based on GPS data. *Earthq Sci* 29:291–298. <https://doi.org/10.1007/s11589-016-0167-y>
- Rakoto V, Lognonné P, Rolland L (2017) Tsunami modeling with solid earth-ocean-atmosphere coupled normal modes. *Geophys J Int* 211(2):1119–1138. <https://doi.org/10.1093/gji/ggx322>
- Rakoto V, Lognonné P, Rolland L, Coïsson P (2018) Tsunami wave height estimation from GPS-derived ionospheric data. *J Geophys Res-Space* 123:4329–4348. <https://doi.org/10.1002/2017JA024654>
- Reymond D, Okal EA, Hébert H, Bourdet M (2012) Rapid forecast of tsunami wave heights from a database of pre-computed simulations, and application during the 2011 Tohoku tsunami in French Polynesia. *Geophys Res Lett* 39:L11603. <https://doi.org/10.1029/2012GL051640>
- Rius A, Aparicio JM, Cardellach E, Martín-Neira M, Chapron B (2002) Sea surface state measured using GPS reflected signals. *Geophys Res Lett* 29:2122–2125. <https://doi.org/10.1029/2002GL015524>
- Roch J, Duperray P, Schindelé F (2016) Very fast characterization of fault parameters through W-phase centroid inversion in the context of tsunami warning. *Pure appl Geophys* 173:3881–3893. <https://doi.org/10.1007/s00024-016-1258-3>
- Roger J, Hébert H, Ruegg J-C, Briole P (2011) The El Asnam October 10th, 1980 inland earthquake: a new hypothesis of tsunami generation. *Geophys J Int* 185:1135–1146. <https://doi.org/10.1111/j.1365-246X.2011.05003.x>
- Rolland LM, Occhipinti G, Lognonné P, Loevenbruck A (2010) Ionospheric gravity waves detected offshore Hawaii after tsunamis. *Geophys Res Lett* 37:L17101. <https://doi.org/10.1029/2010GL044479>
- Rolland LM, Lognonné P, Astafeyeva E, Kherani EA, Kobayashi N, Mann M, Munekane H (2011) The resonant response of the ionosphere imaged after the 2011 off the Pacific coast of Tohoku Earthquake. *Earth Planets Space* 63(7):853–857. <https://doi.org/10.5047/eps.2011.06.020>
- Rolland LM, Vergnolle M, Nocquet J-M, Sladen A, Dessa J-X, Tavakoli F et al (2013) Discriminating the tectonic and non-tectonic contributions in the ionospheric signature of the 2011, Mw 7.1, dip-slip Van earthquake, Eastern Turkey. *Geophys Res Lett* 40(11):2518–2522. <https://doi.org/10.1002/grl.50544>

- Ruffini G, Soulat F, Caparrini M, Germain O, Martín-Neira M (2004) The Eddy experiment: accurate GNSS-R ocean altimetry from low altitude aircraft. *Geophys Res Lett* 31:L12306. <https://doi.org/10.1029/2004GL019994>
- Salameh E, Frappart F, Almar R, Baptista P, Heygster G, Lubac B, Raucoules D, Almeida LP, Bergsma EWJ, Capo S, de Michele M, Idier D, Li Z, Marieu V, Poupardin A, Silva PA, Turki I, Laignel B (2019) Monitoring beach topography and nearshore bathymetry using spaceborne remote sensing: a review. *Remote Sens* 11:2212. <https://doi.org/10.3390/rs11192212>
- Satake K (1988) Effects of bathymetry on tsunami propagation: application of ray tracing to tsunamis. *Pure Appl Geoph*. <https://doi.org/10.1007/BF00876912>
- Savastano G, Komjathy A, Verkhoglyadova O, Mazzoni A, Crespi M, Wei Y, Mannucci AJ (2017) Real-time detection of tsunami ionospheric disturbances with a stand-alone GNSS receiver: a preliminary feasibility demonstration. *Sci Rep* 7:46607. <https://doi.org/10.1038/srep46607>
- Sladen A, Hébert H (2008) On the use of satellite altimetry to infer the earthquake rupture characteristics: application to the 2004 Sumatra event. *Geophys J Int* 172(2):707–714. <https://doi.org/10.1111/j.1365-246X.2007.03669.x>
- Sladen A, Rivet D, Ampuero JP et al (2019) Distributed sensing of earthquakes and ocean-solid Earth interactions on seafloor telecom cables. *Nat Commun* 10:5777. <https://doi.org/10.1038/s41467-019-13793-z>
- Smith WHF (1993) On the accuracy of digital bathymetric data. *J Geophys Res* 98(B6):9591–9603. <https://doi.org/10.1029/93JB00716>
- Smith WHF, Sandwell DT (1997) Global seafloor topography from satellite altimetry and ship depth soundings. *Science* 277:1956–1962. <https://doi.org/10.1126/science.277.5334.1956>
- Smith SM, Martinis CR, Baumgardner J, Mendillo M (2015) All-sky imaging of transglobal thermospheric gravity waves generated by the March 2011 Tohoku earthquake. *J Geophys Res Space Phys* 120:10992–10999. <https://doi.org/10.1002/2015JA021638>
- Song YT, Fukumori I, Shum CK, Yi Y (2012) Merging tsunamis of the 2011 Tohoku-Oki earthquake detected over the open ocean. *Geophys Res Lett* 39:L05606. <https://doi.org/10.1029/2011GL050767>
- Stosius R, Beyerle G, Helm A, Hoechner A, Wickert J (2010) Simulation of space-borne tsunami detection using GNSS-Reflectometry applied to tsunamis in the Indian Ocean. *Nat Hazards Earth Syst* 10:1359–1372. <https://doi.org/10.5194/nhess-10-1359-2010>
- Stosius R, Beyerle A, Hoechner A, Wickert J, Lauterjung J (2011) The impact on tsunami detection from space using GNSS-reflectometry when combining GPS with GLONASS and Galileo. *Adv Space Res* 47:843–853. <https://doi.org/10.1016/j.asr.2010.09.022>
- Synolakis CE, Bernard EN (2006) Tsunami science before and beyond Boxing Day 2004. *Philos Trans R Soc A* 364:2231–2265. <https://doi.org/10.1098/rsta.2006.1824>
- Terada, Y, Kato T, Nagai T, Koshimura S, Imada N, Sakaue H, Tadokoro K (2015) Recent developments of GPS tsunami meter for a far offshore observations. In: Hashimoto M (ed) International symposium on geodesy for earthquake and natural hazards (GENAH). International Association of Geodesy Symposia, Springer, Cham. https://doi.org/10.1007/1345_2015_151
- Thomson R, Fine I, Rabinovich A, Mihály S, Davis E, Heesemann M, Krassovski M (2011) Observation of the 2009 Samoa tsunami by the NEPTUNE-Canada cabled observatory: test data for an operational regional tsunami forecast model. *Geophys Res Lett* 38:L11701. <https://doi.org/10.1029/2011GL046728>
- Tinti S, Manucci A, Pagnoni G, Armigliato A, Zaniboni F (2005) The 30 December 2002 landslide-induced tsunamis in Stromboli: sequence of the events reconstructed from the eyewitness accounts. *Nat Hazard Earth Syst* 5:763–775. <https://doi.org/10.5194/nhess-5-763-2005>
- Titov VV (2009) Tsunami forecasting. In: Bernard EN, Robinson AR (eds) *The sea*, vol 15. Harvard University Press, Cambridge, pp 371–400
- Titov VV, González FI (1997) Implementation and testing of the method of splitting tsunami (MOST) model. Technical report NOAA Tech. Memo. ERL PMEL-112 (PB98-122773) NOAA/Pacific Marine Environmental Laboratory Seattle, WA
- Titov VV, González FI, Bernard EN, Eble MC, Mofjeld HO, Newman JC, Venturato AJ (2005) Real-time tsunami forecasting: challenges and solutions. *Nat Hazard* 35(1):41–58. <https://doi.org/10.1007/s11069-004-2403-3>
- Tsushima H, Hino R, Ohta Y, Iinuma T, Miura S (2014) tFISH/RAPiD: rapid improvement of near-field tsunami forecasting based on offshore tsunami data by incorporating onshore GNSS data. *Geophys Res Lett* 41:3390–3397. <https://doi.org/10.1002/2014GL059863>
- Uma Devi E, Sunanda V, Ajay Kumar B, Patanjali Kumar Ch, Srinivasa Kumar T (2016) Real-time earthquake monitoring at the Indian Tsunami Early Warning System for tsunami advisories in the Indian Ocean. *Int J Ocean Clim Syst* 7(1):20–26. <https://doi.org/10.1177/1759313115623164>
- UNESCAP (UN Economic and Social Commission for Asia and the Pacific) (2019) Roundtable: maritime sector strategies to augment Tsunami monitoring with economic, safety and environmental

- co-benefits. Roundtable, 22–23 Aug 2019. <https://www.unescap.org/sites/default/files/Roundtable%20Outcome%20Report%20April%202020.pdf>. Accessed August 2020
- Vadas SL, Makela JJ, Nicolls MJ, Milliff RF (2015) Excitation of gravity waves by ocean surface wave packets: upward propagation and reconstruction of the thermospheric gravity wave field. *J Geophys Res Space Phys* 120:9748–9780. <https://doi.org/10.1002/2015JA021430>
- Vallée M, Ampuero J-P, Juhel K, Bernard P, Montagner J-P, Barsuglia M (2017) Observations and modeling of the elastogravity signals preceding direct elasticity waves. *Science* 358(6367):1164–1168. <https://doi.org/10.1126/science.aao0746>
- Walker JG (1984) Satellite constellations. *J Br Interplanet Soc* 37:559–571
- Wang R, Parolai S, Ge M, Jin M, Walter TR, Zschau J (2013) The 2011 Mw 9.0 Tohoku Earthquake: comparison of GPS and strong-motion data. *Bull Seismol Soc Am* 103:1336–1347. <https://doi.org/10.1785/0120110264>
- WMO (2018) Manual on the global telecommunication system, annex III to the WMO technical regulations, 2015 Edition, updated in 2018, 200 pp
- Yamamoto N, Hirata K, Aoi S, Suzuki W, Nakamura H, Kunugi T (2016) Rapid estimation of tsunami source centroid location using a dense offshore observation network. *Geophys Res Lett* 43:4263–4269. <https://doi.org/10.1002/2016GL068169>
- Yan X, Sun Y, Yu T, Liu J-Y, Qi Y, Xia C et al (2018) Stratosphere perturbed by the 2011 Mw9.0 Tohoku earthquake. *Geophys Res Lett* 45(10):10050–10056. <https://doi.org/10.1029/2018GL079046>
- Yang Y-M, Verkhoglyadova O, Mlynchak MG, Mannucci AJ, Meng X, Langley RB, Hunt LA (2017) Satellite-based observations of tsunami-induced mesosphere airglow perturbation. *Geophys Res Lett* 44:522–532. <https://doi.org/10.1002/2016GL070764>
- Yang Y, Dunham EM, Barnier G, Almqvist M (2019) Tsunami wavefield reconstruction and forecasting using the ensemble Kalman filter. *Geophys Res Lett* 46:853–860. <https://doi.org/10.1029/2018GL080644>
- Ye L, Kanamori H, Rivera L, Lay T, Zhou Y, Sianipar D, Satake K (2020) The 22 December 2018 tsunami from flank collapse of Anak Krakatau volcano during eruption. *Sci Adv*. <https://doi.org/10.1126/sciadv.aaz1377>
- Yu Y, Wang W, Hickey MP (2017) Ionospheric signatures of gravity waves produced by the 2004 Sumatra and 2011 Tohoku tsunamis: a modeling study. *J Geophys Res Space Phys* 122:1146–1162. <https://doi.org/10.1002/2016JA023116>

Publisher's Note Springer Nature remains neutral with regard to jurisdictional claims in published maps and institutional affiliations.

Affiliations

H. Hébert¹  · G. Occhipinti² · F. Schindelé¹ · A. Gailler¹ · B. Pinel-Puysségur¹ · H. K. Gupta³ · L. Rolland⁴ · P. Lognonné²  · F. Lavigne⁵ · E. Meilianda⁶ · S. Chapkanski⁵ · F. Crespon⁷ · A. Paris¹ · P. Heinrich¹ · A. Monnier¹ · A. Jamelot⁸ · D. Reymond⁸ 

¹ CEA, DAM, DIF, 91297 Arpajon Cedex, France

² Université de Paris, Institut de Physique du Globe de Paris, CNRS, 75005 Paris, France

³ CSIR-National Geophysical Research Institute, Uppal Road, Hyderabad 500007, India

⁴ OCA, CNRS, IRD, Géoazur, Université Côte d'Azur, 06560 Valbonne, France

⁵ Laboratoire de Géographie Physique UMR 8591, Université Paris 1 Panthéon-Sorbonne, 1 Place Aristide Briand, 92195 Meudon, France

⁶ Tsunami and Disaster Mitigation Research Center (TDMRC), Syiah Kuala University, Jalan Prof. Dr. Ibrahim Hasan, Ulee Lheue, Kecamatan Meuraxa, Banda Aceh 23232, Indonesia

⁷ Noveltis, 31672 Labège, France

⁸ LDG/Pamatai, Papeete, Tahiti 98713, French Polynesia

Terms and Conditions

Springer Nature journal content, brought to you courtesy of Springer Nature Customer Service Center GmbH (“Springer Nature”).

Springer Nature supports a reasonable amount of sharing of research papers by authors, subscribers and authorised users (“Users”), for small-scale personal, non-commercial use provided that all copyright, trade and service marks and other proprietary notices are maintained. By accessing, sharing, receiving or otherwise using the Springer Nature journal content you agree to these terms of use (“Terms”). For these purposes, Springer Nature considers academic use (by researchers and students) to be non-commercial.

These Terms are supplementary and will apply in addition to any applicable website terms and conditions, a relevant site licence or a personal subscription. These Terms will prevail over any conflict or ambiguity with regards to the relevant terms, a site licence or a personal subscription (to the extent of the conflict or ambiguity only). For Creative Commons-licensed articles, the terms of the Creative Commons license used will apply.

We collect and use personal data to provide access to the Springer Nature journal content. We may also use these personal data internally within ResearchGate and Springer Nature and as agreed share it, in an anonymised way, for purposes of tracking, analysis and reporting. We will not otherwise disclose your personal data outside the ResearchGate or the Springer Nature group of companies unless we have your permission as detailed in the Privacy Policy.

While Users may use the Springer Nature journal content for small scale, personal non-commercial use, it is important to note that Users may not:

1. use such content for the purpose of providing other users with access on a regular or large scale basis or as a means to circumvent access control;
2. use such content where to do so would be considered a criminal or statutory offence in any jurisdiction, or gives rise to civil liability, or is otherwise unlawful;
3. falsely or misleadingly imply or suggest endorsement, approval, sponsorship, or association unless explicitly agreed to by Springer Nature in writing;
4. use bots or other automated methods to access the content or redirect messages
5. override any security feature or exclusionary protocol; or
6. share the content in order to create substitute for Springer Nature products or services or a systematic database of Springer Nature journal content.

In line with the restriction against commercial use, Springer Nature does not permit the creation of a product or service that creates revenue, royalties, rent or income from our content or its inclusion as part of a paid for service or for other commercial gain. Springer Nature journal content cannot be used for inter-library loans and librarians may not upload Springer Nature journal content on a large scale into their, or any other, institutional repository.

These terms of use are reviewed regularly and may be amended at any time. Springer Nature is not obligated to publish any information or content on this website and may remove it or features or functionality at our sole discretion, at any time with or without notice. Springer Nature may revoke this licence to you at any time and remove access to any copies of the Springer Nature journal content which have been saved.

To the fullest extent permitted by law, Springer Nature makes no warranties, representations or guarantees to Users, either express or implied with respect to the Springer nature journal content and all parties disclaim and waive any implied warranties or warranties imposed by law, including merchantability or fitness for any particular purpose.

Please note that these rights do not automatically extend to content, data or other material published by Springer Nature that may be licensed from third parties.

If you would like to use or distribute our Springer Nature journal content to a wider audience or on a regular basis or in any other manner not expressly permitted by these Terms, please contact Springer Nature at

onlineservice@springernature.com